NTNU
Norwegian University of
Science and Technology

DEPARTMENT OF PHYSICS

MASTER THESIS

# Thermal conductivity of low-dimensional systems

*Author:*
Arne Kristian Kramprud Hjelt

*Supervisor:*
Raffaela Cabriolu

December, 2022

# Abstract

Being able to tailor the thermal properties of a material for a specific application is a widely desired technological feature. Thermal conductivity (TC), in particular, measures the ability of a material to conduct or transport heat, and it is considered an intensive property of the material. Despite the enormous implications, the thermal transport process is not fully understood yet. Furthermore, many theoretical and experimental works have reported for quasi-1-dimensional (1D) objects, an anomalous strong dependence of the thermal conductivity on the system size, breaking the intensive character of this thermal property. In this work, I have studied the effect of dimensionality on Graphene. The unusually high thermal conductivity of Graphene in certain conditions gives it a huge potential for technological application. In this thesis, I address the dimensionality effect of Graphene by means of molecular dynamics simulations using the "approach to equilibrium molecular dynamics" (AEMD) technique. My simulations have been able to reproduce the data from a reference paper, and have shown that, according to some other theoretical and experimental findings, the TC depends on the shape of the edge-configuration if we reduce the width of the 2D graphene sample to a quasi-1D object. In general, the TC for graphene low dimensional systems, such as ribbons, decreases respect to the value measured for the bulk Graphene.

# Sammendrag

Å kunne designe materialer slik at de får optimale termiske egenskaper er svært ettertraktet innen mange teknologiske fagfelt. Termisk konduksjon, også kalt varmeledningsevne, er en intensiv egenskap ved et materie, og utnyttes aktivt i mange moderne teknologiske produkter, som for eksmpel i smarttelefoner. Fremskritt innen varmeledning har store konsekvenser. Tross dette, er ikke termisk konduksjon et ferdig utviklet fagfelt.

Spessielt når man beveger seg ned mot nano nivå og studerer kvasi-en-dimensjonale (1D) objekter, blir det klassisket bildet av termisk konduksjon som en intensiv egenskap, utfordret. Dette fordi varmeledningsevnen til slike objekter ser ut til å uventet sterkt koblet til systemet størrelse, noe som bryter med at ideen om at det er en utelukket intensiv egenskap.

I denne masteroppgaven har brukt "Molecular-Dynamics" og en metode some heter "Approach to Equilibrium Method" til å simulere tynne strimler med grafen for å finne ut hvor fort de leder varme. Jeg har har studert strimler som har mellom 1 og 9 heksagonale karbon strukturer i bredden. Dette er interssant å utforske fordi andre målinger av de termiske egenskapene til grafen har vist at dette materialet har et enormt potensiale til å lede varme. Å kunne utnyttet dette potensiale til det fulle vil kreve mere forskning, og mine arbeider inngår i den videre kartlegging av hvordan grafen leder varme. Gjennom simuleringene i denne oppgaven har jeg klart å gjenskape data fra en referanseartikkel, noe som gir meg en bekreftelse på at jeg har forstått og implementert metodene jeg bruker korrekt. Funnen mine peker mot at den termiske konduksjonen i grafen strimler avhenger av hvordan kanten på lengdreretningen til strimlene ser ut. Generelt er resultatene for varmeledningsevnen til strimlene lavere enn resultatene for større segmenter undersøkt i andres arbeider.

Arbeidet har blitt veiledet av Raffaela Cabriolu.

# Contents

# Abbreviations

AEMD - Approach to Equilibrium Molecular Dynamics
MD - Molecular Dynamics
LAMMPS - Large-scale Atomic/Molecular Massively Parallel Simulator
GNR - Graphene Nano Ribbon
AGNR - Graphene Nano Ribbon built in the armchair orientation (3.9)
ZGNR - Graphene Nano Riobbon built in the zigzag orientation (3.10
Strip - a single string of carbon atoms that stacked on top of eachother builds up the GNR's
TC - Thermal Conductivity
TD - Thermal Diffusivity
NEMD - Non Equilibrium Molecular Dynamics
EMD - Equilibrium Molecular Dynamics

# Chapter 1

# Introduction and Background

This chapter gives a brief overview and motivation for the scientific topic I have explored in my master's thesis work. Objectives and a description of this thesis are also included.

## 1.1 Introduction

Thermal conductivity (TC) is the physical property that measures the rate of heat transfer through a material by conduction or diffusion process, and, it is one of the most difficult properties to measure, either experimentally or by computation. Understanding and manipulating TC is crucial for optimizing performance, efficiency, and overall energy usage in industries and everyday life. Indeed thermal management of small electronics equipment (i.e. mobile phones laptops, house appliances, etc..), heat exchange in industrial systems (i.e. chemical, automotive, aerospace industries, etc ...), and insulation in buildings are only a few examples that testify to the importance of the topic in today's global climate crisis solutions for which the minimization of carbon emissions requires the reduction of abnormal energy consumption and heat waste.[1] Depending on the applications in mind, high or low-thermal conductivity materials are desirable to move or block heat. Solid-state lighting, transistors, high-performance optical devices, batteries, energy storage, and carbon-capture materials require high thermal conductivity to quickly and efficiently dissipate heat that could otherwise damage the device or impair important physical processes and reactions. On the other hand, low thermal conductivity materials are widely needed to build thermal coatings for gas turbine systems, for thermoelectric devices, and to minimize heat transfer across heat pumps, refrigerators, and air conditioning.[2] Thermal conductivity is defined by the phenomenological Fourier's law (section 2) of heat conduction, and is an intrinsic property of the material, however, for systems with lower dimensions, a surprisingly anomalous thermal conductivity that depends on the sample size is observed.[3]

Graphene is a two-dimensional (2D) material with extraordinary optical, mechanical, chemical, electrical, and thermal conductivity qualities, and it is one of

the most investigated materials in the previous decades.[4] Since the first time freestanding graphene was successfully synthesized with the exfoliation or "stick and pencil method", [5] graphene is used in electronics, energy storage, sensors coatings, composites for solar cells, biomedical devices and many other. Its high surface area and biocompatibility make it attractive also as a material for drug delivery and tissue engineering applications. Graphene has an exceptionally high thermal conductivity, that has been measured to reach up to $4000 W m^{-1} K^{-1}$ in certain conditions.[4] Furthermore, its discovery provided also the possibility to study experimentally the heat transport in low-dimension systems. As expected by theoretical predictions, reduced dimensionality systems display very different thermal transport behavior compared to the three-dimensional bulk counterpart.[3] Indeed, in a non-metallic system the carriers of heat are phonons, i.e. quantized lattice vibrations, of which their density is deeply affected by the symmetry and dimensionality of the system. Furthermore, another signature of thermal conductivity appears also in quasi-one-dimensional systems, for which a diverging thermal conductivity is observed.

In this thesis, I have calculated the thermal conductivity of an initial Graphene sample using the Approach to Equilibrium Molecular Dynamics technique,[6, 7] and compared my results with data coming from previous literature,[8]. In the second part of the thesis, I studied the effect of dimensionality on the thermal conductivity progressively reducing one dimension until the 2D sample would have reached the quasi-1D system configurations. The results are comparable with previous literature and findings.

## 1.2 Motivation of the work

This section contains the main aim and a list with a short description of the objectives I intended to reach with this master thesis.
**The main aim** of this study was the investigation of the size effect on the TC of Graphene. To reach my main aim I have divided my work in different objectives:

- *Objective 1: Implementation of AEMD in LAMMPS.* To be able to calculate the thermal conductivity, I had to get acquainted with the Approach to Equilibrium Molecular Dynamics (AEMD) method in the LAMMPS MD engine. This step has not been easy because it contained a series of no trivial subsets. I have created by myself the Graphene samples and I have implemented the input files in LAMMPS with the AIREBO potential. After those preliminary tests and an understanding of the thermal conductivity theoretical background, I have also implemented the AEMD algorithm in LAMMPS.
- *Objective 2: Reproducing MD literature data.* I have dedicated a few months to testing the computation of the TC and finally, I have been able to reproduce the value of the Thermal conductivity in the paper by Barbarino et al. [8]. This step was quite long but give me the confidence that my LAMMPS input file and the post-processing programs were correct.

- *Objective 3: Production work for the thesis.* Finally, I have dedicated most of my thesis time to performing the core simulation experiments of my thesis. I have considered an initial Graphene sample with dimension $2030nm \times 2.2nm$ and decreased the thickness of the 2D initial configuration to create thinner and thinner samples until I have reached the quasi-1D sample.

## 1.3 Description of my master thesis

This master project focuses on the investigation of the size effect on the thermal conductivity considering a 2D layer of Graphene that has been progressively reduced to a quasi-1D object stripping the layers of chains from it. This report is organized as follows: Chapter 1 gives an introduction to this work, outlines the motivation for it and describes its composition; Chapter 2 presents an introduction to molecular simulation and the scientific topic; Chapter 3 briefly introduces the chosen computational method, Molecular Dynamics (MD), and the computational technique to calculate the TC, i.e. Approach to Equilibrium MD (AEMD), together with descriptions of some of the challenges, and how I chose to overcome them; Chapter 4 presents my results compared to the ones of the original papers, and, the calculation of TC for Graphene and for the quasi-1D sample; Finally, Chapter 5 outlines the conclusions of this thesis.

# Chapter 2

# Theoretical and Scientific Background

In the past decades, there has been an incredible fast progress in the design, manufacturing and applications of different electronic device. However, still there is a lack of theoretically understanding and predicting of how those devices transfer heat, and this impedes the optimal exploitation of them. The main challenge to understand thermal transport in dielectrics, for example, is due to the fact that different length and time scales are involved in the process. Indeed, is well known that the thermal transport in dielectrics is due to "quantized lattice vibrations" or phonon, while the experiments are conducted in the real space and at the macroscale. Therefore, a comprehensive model for those materials would need to refer to a phonon space (atomistic scale), and, at the same time, to the real space of experiments performed at the macroscopic scale. My thesis concerns thermal transport in low-dimensional materials, such as Graphene. In this chapter, I will briefly outline the basics of thermal transport conduction in dielectrics that are needed to investigate the topic of thermal transport in low-dimension materials.

## 2.1 Heat Transport

Heat is the flow of energy transferred from hot to cold regions in agreement with the second law of thermodynamics, and by three different processes; radiation, convection and conduction. With thermal radiation scientists indicate the thermal energy transferred through electromagnetic waves. Convection instead refers to the transfer of heat through masses of fluids, i.e. liquid or gas, that moving transfer heat from the different regions. Conduction is the thermal energy being transferred by the interchanging of kinetic energy between atoms and molecules by direct contact, and, it requires a medium/matter to happen. Since temperature at any point is related to the kinetic energy of the particles, the exchange of kinetic energy will lead to a transfer of heat between them. In addition, temperature also affects the translational, rotational and vibrational motion of the atoms and

molecules [9].

The theory of heat transfer by conduction was first published by Joseph Fourier in 1822, and it is based on the the following empirical formula:

$$\vec{q} = -\mathbf{k}\nabla T \tag{2.1}$$

This equation states that the heat flux due to conduction, $\vec{q}$, is proportional to the gradient of the temperature applied to the sample, $\nabla T$, and opposite to it in sign [10]. The constant of proportionality, $\mathbf{k}$, is called *thermal conductivity* and it is a second order tensor. The heat flux, $\vec{q}$, or rate of flow per unit area is measured in S.I. as $W/m^2$, and, for a cubic isotropic material has components:

$$q_x = -k_{xx}\frac{dT}{dx},\ q_y = -k_{yy}\frac{dT}{dy},\ q_z = -k_{zz}\frac{dT}{dz} \tag{2.2}$$

In an isotropic material $k_{xx} = k_{yy} = k_{zz}$, and the off diagonal components of the $\mathbf{k}$ tensor are approximately null, therefore the thermal conductivity reduces to a scalar, $k$, measured in S.I. as $W/(mK)$. However, in a crystal structure with different axis of symmetry the thermal conductivity depends on the direction to which the thermal gradient is applied to. Since variations in the internal structure affects the diffusion of heat, also the temperature and pressure in a material affects $k$. Solid materials with a lattice structure often display only small variations in $k$ over temperature ranges of hundreds of kelvin, however there are differences between materials. A material like platinum has $\Delta k < 10W/(mK)$ over a span from $-200°C$ to $+1000°C$ , while a material like brass will double its thermal diffusivity from $-200°C$ to $+200°C$ [10].

It is interesting to understand how the empirical macroscopic theory of Fourier reconciles with the an atomistic model of crystal. Heat transport by conduction happens through electrons, photons, phonons, atoms, or molecules. Specifically in the case of electrical insulators materials, or dielectrics, such as graphene, the electronic and photonic contributions can be neglected at low temperature and the phonon contributions dominates the TC. In solid-state physics, the harmonic theory of crystal approximates the lattice as a coupled mass and spring system, following the main assumptions that the mean equilibrium positions of each atom are the Bravais lattice site and that the displacements of atoms from their equilibrium positions are small compared with the interionic spacing. The harmonic approximation is the starting point for all the theories of lattice dynamics arguing that thermal energy can be stored as excited vibrational normal modes of the crystal, i.e. phonons [11]. However, the harmonic theory is exact only a zero temperature, therefore cannot describe heat transport, that, according to Fourier's Law depends on the gradient of the Temperature. Anharmonicity, or higher-order terms in the harmonic approximation of lattice must be considered for the heat transfer to happen by diffusion process. Indeed, in this picture, heat transport by conduction in dielectrics happens because of different "scattering" mechanisms among phonons instead of the simple picture of a phonon that ballistically cross the sample with a straight path without deflections. Three different scattering

mechanisms are suggested [12], phonon-phonon scattering, phonon-defect scattering and phonon-boundary scattering. The random nature of the conductivity is described by the temperature gradient, in the Fourier's law, and, from that law, it is easy to recover the Debye expression on the thermal conductivity for cubic materials:

$$k = \frac{1}{3} \int C_v(\omega) v(\omega) l(\omega) d\omega \tag{2.3}$$

where $C_v$ is the phonon heat capacity per unit volume, $v$ is the phonon group velocity, and $l$ represents the mean free path of the phonon. In the above formula, the "scalar" thermal conductivity is obtained by summing over each vibration frequency $\omega$. The above formula also assesses the importance of the average mean free path of phonons, which is described as the distance over which a phonon travels before the consecutive scattering. To have the intrinsic bulk thermal conductivity, the dimension of the investigated sample must be such to include the average mean free path of the phonons and avoid an underestimation of the thermal conductivity. The discussion up to now refers to thermal transport in dielectric three-dimensional crystals, and, a part of the phonon particle nature, it is mainly a classical picture. This picture is not valid for all the materials, and over the years, many alternatives have been suggested to include quantum effects into the picture [13], however, the transport process is not fully understood and cannot be easily predicted for all the materials. The intrinsic character of the thermal conductivity, for example, seems to vanish for low-dimensional materials, such as Graphene and quasi-1D materials.

### 2.1.1 Methods to measure Thermal conductivity

Measuring TC has its own intrinsic limitations, especially for crystal insulators, for which the process, is dominated by phonon scattering. The challenges are different depending if you use experimental, theoretical or modelling methods. In this section, I will outline the experimental, theoretical and, only briefly, the modelling methods. I will treat in details the modelling methods in Chapter 3.

#### Experiments

Traditionally, direct experimental techniques [3, 10, 14] are based on the application of the Fourier law for 1-dimensional system and consist of establishing a steady-state heat flux through the sample connected from one side to a heat sink and from the other one to a heat source, see sketch in figure 2.1.

From the resulting constant temperature gradient ($\Delta T$) provided by thermocouples, the measure of the heat flow ($q$) and the dimension of the sample, $\Delta x$, the TC is directly obtained by Eq.2.2. However, this approach includes inevitably contributions to the heat transfer by convection and radiation process, while TC is a parameter that refers only to the pure conduction phenomena. Additionally,

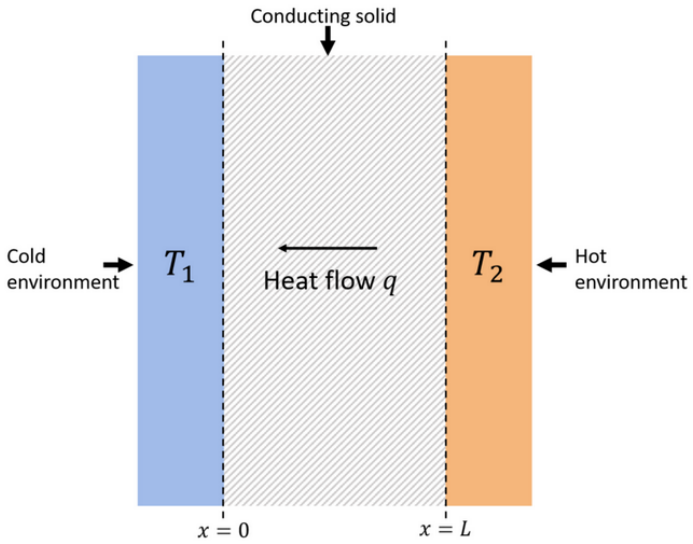


**Figure 2.1:** Sketch that models the connection between the experiments and the Fourier's law 2.2.

the application of the Fourier law requires a heat flow propagating along one dimension, while in practice, during experiments, is almost impossible to limit the two-dimensional heat flow, and, finally, because TC is temperature-dependent, particular care is required in the choice of the temperature range of the heat bath and sink of the setup. The comparative method [14] borrows the idea of the steady state method described above, and adds a reference material between the source and sink, and next to test sample. The known properties of the reference material allow to know the TC the unknown specimen by comparison. Eq. 2.2 still applies, and the comparison of the temperature behavior of the reference material to the temperature behavior of the test sample provides a more certain measurement of thermal conductivity [14]. However, the added component to the stack increases the sources of heat loss to account for, making the accuracy of the measurement depend more strongly on the certainty of the reference material properties. Other more complex methods are also available to measure thermal conductivity, including the radial flow method, the laser-flash diffusivity method, and the pulse-power method [14]. The radial flow method involves circular or cylindrical geometry with an internal heat source. This method greatly minimizes the thermal radiation loss radially, since the supplied heat flow is also radial. The drawback to this method is that it requires rather large sample sizes which may not be feasible to obtain for research materials. The laser-flash diffusivity method calculates the thermal diffusivity of a material. One face of a sample is irradiated by a short laser pulse, and the temperature response of the opposite face is recorded. The temperature rise versus time profile is used to calculate thermal diffusivity, and if the density and specific heat are known, thermal conductivity can be calculated. The advantage of this method is the short test time, as waiting for

steady state is not an issue. However, the sample requirements can be strict, since the sample surfaces must have a high absorptivity. The pulse-power method uses a current pulse supplied to a heater through a sample. This is another transient method, not requiring steady state. This method is commercially used because of its accuracy.

**Theoretical methodes**

An alternative way to calculate the thermal conductivity is to solve the exact "Boltzmann Transport Equation" ( BTE) for phonons using the phonon-phonon collision rates obtained combining Density Functional Theory (DFT) and lattice dynamics [15]. The BTE is a non linear integro-differential equation and its solution is thus a difficult problem. Therefore, scientists have to resort to some simplification and one of the obvious simplifications is to linearize the BTE to obtain the phonon heat flux by summing over all the phonon modes. The workflow can be described as the following. DFT calculations can provide atomic force constants from empirical and/or first principle potentials that are fitted to reproduce thermal transport-related properties. In a second stage, the phonon frequencies from lattice dynamics are used to exactly solve the linear-BTE (LBTE). Fundamental for this theory is the taking into account of the intrinsic and extrinsic lifetime calculations that are included in the anharmonic lattice dynamic and perturbation theory that are essential for the solutions of the LBTE. The intrinsic phonon lifetimes is measuring the lifetime of a phonon mode, i.e. is related to the scattering of phonons with other phonons. This fundamental part is calculated based on a perturbation to the non-interacting harmonic modes. Furthermore, a combination of the BTE with the empirical Fourier's law provide a way to calculate directly the thermal conductivity. Successful calculations have predicted thermal conductivity of semiconductor and other materials [3, 15] providing that the initial force constants and/or DFT calculations on potentials fitted to reproduce thermal properties.

**Modelling**

On the other hand, molecular simulations are very popular since are the ideal tool to reveal the mechanism of phonons thermal transport at the atomistic and molecular scale and can naturally go from the phonon description, i.e. the reciprocal space, to the real space in its implementation. TC is determined mainly by the modes arising from bending and especially torsions, whose energy is comparable or less to that one of room temperature, at which a classical description is enough. These arguments justify the usage of the classical molecular techniques, such as Molecular Dynamics (MD), to calculate TC respect to electronic-based modelling methods, i.e. Density Functional Theory (DFT). The two most common approaches for predicting phonon (i.e. lattice) thermal conductivity using MD simulation are the Green-Kubo (GK) and direct methods (DMs), i.e. Non-Equilibrium

Molecular Dynamics methods. In my work I have used a non equilibrium method that I will explain in more details in Chapter 3.

## 2.2 Thermal conductivity of low dimensional material

It is known that the dimensionality reduction deeply affect the thermal properties of materials [3], since the symmetry, the density of phonon states, the boundaries and the scattering process are very different with respect to the bulk counterpart. However, the way in which the dimensionality affects the thermal conductivity is unknown and it remains a debate for different materials. The successful synthesis of Graphene provides the ideal field-camp to test the theories and understanding of thermal conductivity in low dimensional materials. Considering that the 2D and quasi 1-D structures would limit the number of scattering events respect to the bulk counterpart, one would expect a very large or even divergent thermal conductivity, on the other hand, the boundary could provide the surface scattering hampering the thermal transport. Experimental on different systems show a very complex behavior in which dimensionality reduction can hamper or boost the thermal conductivity depending on the system and on the experimental technique used [3]. Very high thermal conductivity has been measured in bulk Graphene [16–20], and in carbon nanotubes, while a suppression of thermal conductivity has been, for example, measured in silicon nanowires and membranes [3]. It is well known that the experimental measures of thermal conductivity on low dimensional material are extremely difficult and sensible to the external conditions, and even if successfully measured the origin of the k suppression or enhancement respect to the bulk counterpart, is not well understood.

Molecular simulations models the process at atomistic scale (see Sec. 3) and allows to bridge the phonon space with the real space. Many simulations with different techniques have tried to probe some experimental findings for 2D or quasi-1D systems. In molecular simulation method [21], the dependence on the dimensionality can be associated to the simulation's cell dimensions which hinders phonons having mean free path (MFP) greater than the actual cell length, $L_x$. In principle, a reliable description of the intrinsic thermal conductivity would need the phonons' motion to achieve the diffusive regime by increasing the simulation cell length up to a critical length called $L_{diff}$ that corresponds to the length at which the phonons' transport becomes diffusive as described by Eq.2.2. However, in different 2D and quasi 1D materials, the intrinsic picture given by Eq.2.2 does not hold [3]. Despite many modelling investigations, up to now, there is no clear evidence of any universal beahvior for 2D and quasi-1D materials. In conclusions, even if both experiments and theory agree on the actual length-dependence for low dimensional systems, an active debate about a possible universal divergence of thermal conductivity for quasi-1D system is still open. In the next section, I will give a scientific background on Graphene and Graphene Nanoribbons thermal conductivity.

### 2.2.1 Graphene and Graphene Nanoribbons

Graphene is a single layer of carbon atoms sp2-bounded in a hexagonal honeycomb lattice with a bond length equal to 0.142 nanometers. Layers of Graphene on top of each other with an inter-planar distance equal to 0.335 nanometers form graphite from which graphene can be "exfoliated" to overcome the van der Waals forces that held them together.

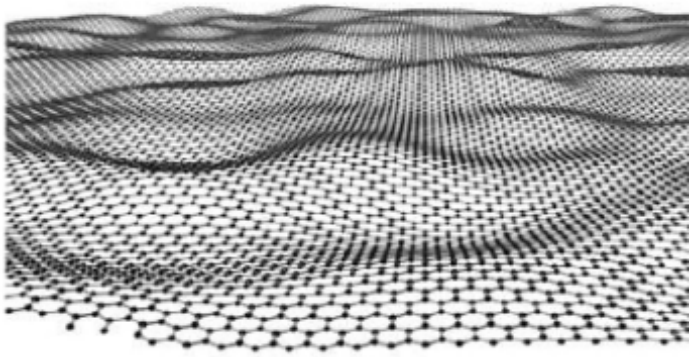

**Figure 2.2:** Graphene layer from ref. [22].

Graphene is the thinnest and lightest material known, $0.77mg$ per $m^2$, it is stronger than steel, i.e. tensile strength 130 GPa, it has exceptional heat and electricity conduction performances, with electron mobility of over $200cm^2/(V \cdot s^{-1})$, and, it has outstanding optical properties. Since the first "mechanical obtainment" of graphene [5], applications within different scientific disciplines have exploded, particularly in high-frequency electronics, bio, chemical and magnetic sensors, ultra-wide bandwidth photodetectors, and energy storage and generation.

It should be said that, a part of Graphene, very few materials are purely 2D in nature, and for this it constitutes the ideal material to test the heat transport in low-dimensional systems. A finite termination of Graphene makes a quasi-1D material or ribbon also called Graphene Nanoribbon (GNR) that can have two different edge geometries, known as zigzg and armchair, as shown in picture 2.3:

There are various theoretical, modelling and experimental studies on those promising GNR. Contrary to the Armchair edge Graphene Nanoribbons (AGNRs), the semiconducting Zig-Zag edge Graphene Nanoribbons (ZGNRs) have been found to have interesting magnetic properties, as the "half-metallicity", according to which the material acts as a conductor or an insulator depending on its spin orientation [23]. This interesting observation stimulated new ideas to achieve metal free magnetism in this class of materials. AGNRs do not show magnetic properties, but their electronic structure can be tuned by various means for better device integrations.

Recently, many attempts have been done to fabricate GNR field effect transistors with possibilities of tuning their properties by selective doping of ZGNRs

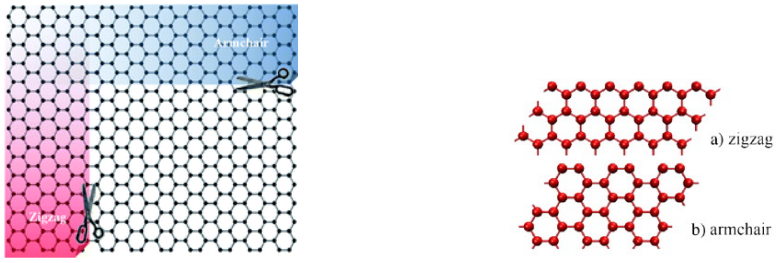


**Figure 2.3:** Zizag and Armchair edge geometries from ref. [23]

and there exist a few experimental studies demonstrating successful fabrication of GNR based devices. All these experimental results show very good agreement with the theoretically predicted band gap values and their width dependence [23]. However, the thermal properties of GNR are still matter of disagreements.

Suspended Graphene has a debated experimental thermal conductivity estimation in the range from 2000 to 8000 $Wm^{-1}K^{-1}$ [3, 16, 22]. GNR have been investigated by modelling and experiments, considering hydrogen passivation in both, ZGNR and AGNR, because theoretical calculations predict saturating graphene edges with hydrogen having a lower energy and form a more stable structure [16]. However, different experimental investigations of whether graphene edges are always hydrogen-terminated were also conducted, and, it has been shown that both graphene edges produced by sputtering in vacuum can exist in a non-functionalized state [24]. Density functional theory revealed similar conclusions, and confirmed the experimentally observed bond contractions attributed to the absence of hydrogen functionalization.

Furthermore, theoretical and modelling work are also showing wide range of values for TC for graphene and graphene nanoribbons. The work from Barbarino et al. [8, 22] studied the thermal conductivity length dependence in pristine graphene (graphene without hydrogen passivation) using "Approach to Non Equilibrium Molecular Dynamics" (AEMD) technique with a "Reactive Empirical Bond Order" (REBO) potential (See Chapter 3). Using a fitting procedure to save computational time, they are providing TC estimation for graphene pristine samples that reach $100\mu m$ size in the direction of the Temperature gradient. The final conclusion is that the TC is upper limited, and there is not diverging TC for graphene pristine. In the paper, the ballistic and diffusive regime are analyzed. In general, the REBO description underestimates the TC of graphene, however, the normalized data of the paper, shows that the obtained TC are in very good agreements with the exact BTE and other previous literature results. This work has been a reference for my thesis, and, I will discuss more thoroughly in chapter 4 where I will show that I have been able to reproduce their data.

In the paper [25] a steady state molecular dynamics approach were used to calculate the thermal conductivity of graphene nanoribbons (GNRs) of several nanometers in size (up to 4 nm wide and 10 nm long). The calculated thermal

conductivity for the zigzag GNR was estimated 2000 W/m-K at 400 K that is a similar order of magnitude of the experimentally measured value for bulk graphene. Furthermore, it was found that nanoribbons with zigzag edges have larger thermal conductivity than nanoribbons with armchair edges, and, that defects as vacancies and edge roughness in the nanoribbons can significantly decrease the thermal conductivity.

More recent experiments [26], reported heat conduction properties of graphene nanoribbons deposited on a silicon carbide substrate. In this study, the graphene nanoribbons have dimensions comparable to or smaller than the phonon mean free path.

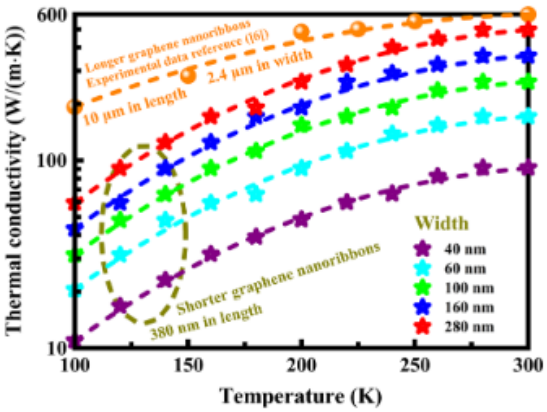


**Figure 2.4:** In-plane thermal conductivity of graphene nanoribbons at different temperatures from ref. [26]. The dimension of the graphene nanoribbons are about 380 nm in length, and the width varies from 40 to 280 nm.

This was done intentionally to investigate the transition from the diffusion to the ballistic thermal transport of the graphene nanoribbons both, experimentally and theoretically. The results indicated that the transport mode of phonons depends grealty upon the length scales of the graphene nanoribbons, and as the dimensions of the graphene nanoribbons decrease, a transition from the diffusive transport mode to the ballistic transport mode was observed. In graph 2.4 from ref.[26], an upper theoretical limit and different results referring to different Nanoribbons width and length are shown. From the graph, it evinces that, as the width of the graphene nanoribbons increases, there is an increase in the thermal conductivity. In this paper, the theoretical values of thermal conductivity were determined on the basis of an equation which defines its dependence on the measured electrical resistance of the opposite thermometer probes. The graph present also the experimental results, which are available from the literature [27], obtained for much longer graphene nanoribbons are also presented for comparison. Also, according to the same reference, the thermal conductivity of graphene nanoribbons depends strongly upon their length and decreases with decreasing the length due to phonon-boundary, as also established in other refer-

ences [28, 29]. Interestingly, there are different papers that found that steady-state or non equilibrium methods applied to GNR exhibit a ballistic transport phenomena, meaning that the scattering to edges or cell boundaries have a dominant contribution for limited sample. Those methods can be applied to study bulk TC if coupled with extrapolation approaches [30]

# Chapter 3

# Computational Methods

To measure the lattice contributions, i.e. phonons, to the thermal conductivity, Molecular Dynamics (MD) simulations constitute the ideal tool because they are able to reveal the mechanism of thermal transport at the atomistic and molecular scale. By simulating graphene at $200-400K$, far below the Debye temperature, the low frequency modes are the dominant contributors to thermal conductivity both in graphene and in GNR's. This justifies the choice of using the classical approach, instead of quantum approaches, in this work.

In the following section I present different computational methods that can be used to obtain the thermal conductivity of graphene. I have only briefly covered the methods that I have not used, i.e. Non-Equilibrium Molecula Dynamics (NEMD) and Green-Kubo method; while I describe in more detail the MD technique and the Approach to Equilibrium MD (AEMD) method that I have used for my thesis.

## 3.1 Molecular Dynamics

Molecular Dynamics (MD) is a statistical mechanics method that integrates Newton's equations of motion to obtain the positions and velocities of atoms and molecules in a system at a given time $t$ [31]. The integration procedure allow for the retrieval of dynamical information as well as the time evolution of the system, something that would otherwise be very hard, or impossible, to obtain at atomistic scale. A typical three-dimensional (3D) simulation system is defined by $N$ particles in an initial configuration at time $t$ such that, for every particle $i$, the corresponding velocity $\mathbf{v}_i(t_0)$ and position $\mathbf{r}_i(t_0)$ are specified inside a simulation box. The velocities are usually set after a Maxwell-Boltzmann distribution such that the total kinetic energy $E_{kin}(t)$ matches a given temperature $T$ according to the following formula:

$$\begin{aligned} E_{kin}(t) &= \sum_{i=1}^{N} \frac{m_i[\mathbf{v}_i(t)]^2}{2} = \frac{3Nk_BT}{2}, \\ [\mathbf{v}_i(t)]^2 &= v_{x,i}^2(t) + v_{y,i}^2(t) + v_{z,i}^2(t), \qquad i = (1,2,...,N). \end{aligned} \tag{3.1}$$

Here the velocity vector $\mathbf{v}_i$ is specified by its components, $v_{x,i}$, $v_{y,i}$ and $v_{z,i}$, the mass of particle $i$ is given by $m_i$, the total number of particles are $N$ and $k_b$ is Boltzmann's constant.

To evolve the system forward in time from $t$ to $t + \Delta t$, the forces on each particle $i$ are derived as the gradients of the potential $V(\mathbf{r}_1, ..., \mathbf{r}_N)$. This potential is a function of the particles positions according to

$$\mathbf{F}_i = -\nabla_{\mathbf{r}_i} V(\mathbf{r}_1, ..., \mathbf{r}_N), \qquad i = (1, 2, ..., N). \tag{3.2}$$

The model for the potential energy defines the interaction between the particles in the simulation cell, and the results depend on the potential we use. There exists different potentials, like the Lennard-Jones potential, Coulomb potential, Morse potential, Buckingham potential, and many more, each with its own strengths and weaknesses. The potential I used is called the Reactive Bond-Order (REBO) potential, that has been shown to be reliable in representing covalent materials, such as silicon and carbon, that form strong directional bonds. I will cover the details of the REBO potential in section 3.5.

Once the total force on each particle has been calculated for the time $t$, the Newton's equations of motion must be solved to obtain the positions and velocities of all the particles at the next time step, $t + \Delta t$. By iteratively solving Newtons equations for each time step, the system evolves forward the desired length in time. The most commonly used integration algorithm in MD is the Verlet algorithm [31, 32] that was introduced in the historical papers [33, 34]. To briefly describe this algorithm, let us consider the evolution of a system by $\Delta t$ time steps. The basic idea of the algorithm is to use the Taylor expansion to express the position $\mathbf{r}(t)$ forward in time, $\mathbf{r}(t + \Delta t)$, and backward in time, $\mathbf{r}(t - \Delta t)$, then adding them together to obtain the following expression;

$$\mathbf{r}(t + \Delta t) = 2\mathbf{r}(t) - \mathbf{r}(t - \Delta t) + \frac{\mathbf{F}(t)}{m_i}\Delta t^2 + O(\Delta t^4) \tag{3.3}$$

It should be said that, when starting at time $t$, the algorithm requires the knowledge of the backward position, i.e. $\mathbf{r}(t - \Delta t)$. This can be obtained by Taylor expansion of degree two, generating an error on the first time step of order $O(\Delta t^3)$, that is a negligible error. This algorithm is simple to implement, while also accurate and stable to run. One could calculate the velocity considering the positions and the mean value theorem [31, 32]; according to

$$\mathbf{v}(t + \Delta t) = \frac{\mathbf{r}(t + \Delta t) - \mathbf{r}(t)}{\Delta t} + O(\Delta t), \tag{3.4}$$

which is a way to approximate the velocity at the cost of accuracy. Some variants of this algorithm have been developed to improve the accuracy issue, i.e. velocity Verlet and leap frog algorithms [32].

To get good results from a molecular dynamics experiment it is important to choose a method that helps explore the phenomena in question. When predicting

phonon (i.e. lattice) thermal conductivity using MD, the two most common approaches are the equilibrium methods, such as Green Kubo, and the Direct Methods (DM) also known as non-equilibrium methods. These will be covered in the next section.

## 3.2 Equilibrium methods for Thermal Conductivity in Molecular Dynamics

The most reliable and rigorous method to calculate Thermal Conductivity in MD simulation is the Green-Kubo (GK). The GK method is an equilibrium MD simulation technique based on the fluctuation-dissipation theorem. According to this theorem, the thermal conductivity tensor is predicted using the fluctuations of the heat flux in equilibrium conditions, or, in other words, calculating the integral of the "Heat Current Auto Correlation Function", $HCACF(t)$, during a standard MD simulation on a cubic cell with periodic boundary conditions. Unfortunately, two aspects make this method challenging. The first one, purely technical, is due to the difficulty of accurately specifying a converged value of the $HCACF(t)$, which often, after a converged region, begins to drift due to noise. For statistical reasons, the accuracy of the $HCACF(t)$ degrades steadily with the increasing value of its argument t. It is difficult to separate, a priori, the interval over which $HCACF(t)$ is computed accurately from the range in which noise is so important to affect the result of the t-integration. Statistical analysis of the error bar is also somewhat uncertain, because of the role of long-time correlations in the MD trajectories. For these reasons, the actual simulation time must greatly exceed the longest lifetime of phonon modes. To force convergence, previous GK computations of TC in crystals resort to running averaging and/or other smoothing methods, which, although very effective, may introduce a bias on the final result whose size is not yet clear. The second challenge is related to the size of the simulation cell, which limits the wavelength of the phonons that reside in the sample, and might affect the estimate of TC in a size dependent manner. This issue is usually addressed by increasing the simulation cell size until the TC becomes size-independent, but this threshold size is not known a priori. On the other hand, the GK method is exact, it is the most rigorous approach up to now, and it allows for the decomposition of the thermal conductivity into contributions associated with acoustic and optical phonons. However, Green-Kubo (GK), requires exceedingly good statistics to give reliable results, and considering the time ahead the GK method is not a good choice of method for the work in my masters thesis, because it would be very computationally demanding.

## 3.3 Non equilibrium methods for Thermal Conductivity calculations

### 3.3.1 Non Equilibrium MD: (NEMD)

The Non Equilibrium MD (NEMD) method is also called a direct method (DM) it recalls the traditional experimental techniques to calculate the thermal conductivity based application of the Fourier law (2.2). A typical implementation of the NEMD method will consist of two themrostat, one at hot tempreature and one at cold temperature, separated by another domain or region. During the MD simulation the temperatures of the thermostats are fixed, while a non equilibrium steady state or temperature gradient is reached in the region between them. Considrineg the temperature $T$ at distance $x$ in the in-between region, both $\frac{\partial T}{\partial x}$ and the average energy transported, $q_x$, are extracted and then used to find the thermal conductivity $k$ according to the Fourier law 2.2. Despite its intuitive appeal, this method normally carries strong non-linear response behaviour, and significant size effects, such that large atomic systems are typically required to obtain an accurate prediction of the bulk phase thermal conductivity. For complex crystals with large unit cells, the computational demands would be enormous. Therefore this ends up not be the choice for my work either.

### 3.3.2 Approach to Equilibrium Molecular Dynamics (AEMD)

A different method to find the thermal conductivity is the Approach to Equilibrium MD method (AEMD). This method was inspired by the flash method, first described in 1960 in [35], where a thin, thermally insulated sample is hit by a laser pulse, while the thermal response, $\Delta T(t)$, is measured on the opposing side. The shape of the curve of the measured $\Delta T(t)$ determines the thermal diffusivity, and the thermal conductivity is calculated as the product of the diffusivity, heat capacity and density. The heat capacity can be calculated by knowing the volume of the sample, the temperature before the pulse hits, the max temperature the sample reaches, and the total energy delivered by the laser pulse. The AEMD protocol exploit a similar approach.

In AEMD the sample is divided into two identical regions, left and right region as in fig. 3.1, each region is separately equilibrated at a different temperature, i.e. left region at $T_{hot}$ and right region at $T_{cold}$. In the sketch, the gradient of temperature is applied to the x direction. After the two regions are separately well equilibrated, they are set into contact and the difference of temperature between them, $\Delta T = T_{left} - T_{right}$, or the profile temperature, is monitored during a standard equilibrium (nve) simulation as the whole sample equilibrate to a common temperature $T$ determining the condition $\Delta T = 0$.

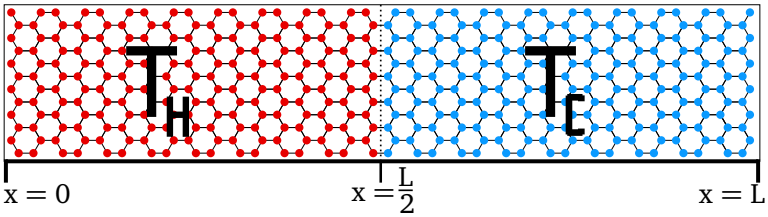


**Figure 3.1:** First stage of AEMD approach, the sample is divided into two identical regions and equilibrated at two different temperature, $T_{left} = T_{hot}$ and $T_{right} = T_{cold}$.

One of the advantages of the AEMD method is that the thermal equilibrium between the two regions is typically reached after $10ps$ to $100ps$, depending on the size of the simulated sample, making this method less computationally demanding than GK and NEMD methods. Another advantage is that there are in general less noise in the results. This is because the temperature is calculated over larger regions, and because the absolute energy flux does not need to be calculated. Heat transport along the x-direction is described by the heat equation

$$\frac{\partial T(t,x)}{\partial t} = \bar{k}\frac{\partial^2 T(t,x)}{\partial x^2} \tag{3.5}$$

where

$$\bar{k} = k/\rho c_v = \frac{kC_v}{V}. \tag{3.6}$$

Here $\bar{k}$ is the thermal diffusivity of the simulated sample with number density $\rho$ $[m^{-3}]$, thermal conductivity $k$ $[WK^{-1}m^{-1}]$, and specific heat $c_v$ $[JK^{-1}]$. $C_v$ is the heat capacity for temperatures above the Debye temperature and $V$ is the volume. We assume that neither $k$, $\rho$ or $c_v$ are dependent on $x$ or $t$ during the duration of the simulation. Using the above equations as a starting point, it is possible to derive ([6][7]) the following equation

$$\Delta T(t) = \sum_{n=1}^{\infty} C_n e^{-\alpha_n^2 \bar{k} t} \tag{3.7}$$

where

$$c_n = 8(T_H - T_C)\frac{[\cos(\alpha_n L/2) - 1]^2}{\alpha_n^2 L^2} \tag{3.8}$$

Here $T_H$ and $T_C$ are the temperatures of the hot and cold region respectively, $\alpha_n = 2\pi n/L$, $L$ is the dimension of the sample to which I apply the gradient (see fig 3.1), $\bar{k}$ is the thermal diffusivity and $t$ is the time.

By fitting the recorded values for $\Delta T(t)$ to equation 3.7, the thermal diffusivity $\bar{k}$ can be calculated, and the thermal conductivity extracted using equation 3.6. This approach works well if we consider temperatures higher than the Debye temperature of the material. However, if the simulated temperature is lower than

the Debye temperature, then a quantum correction factor, $\bar{q}$, has to be introduced into equation 3.6, giving it the final form

$$k = \bar{q}\frac{\bar{k}3NK_B}{V} \tag{3.9}$$

Here $k$ is the thermal conductivity, $\bar{k}$ is the thermal diffusivity, $N$ is the number of atoms, $K_B$ is the Boltzmann constant, $V$ is the volume and $\bar{q}$ is the quantum correction. In the formula, the Dulong-Petit law has been used to write the heat capacity in terms of $N$ and $K_B$. This is because in classical MD simulations all the vibrational degrees of freedom are excited at any temperature since the energy is distributed by the Maxwell-Boltzmann distribution instead of the Bose-Einstein distribution. Therefore the MD simulations only represents reality well when the temperature simulated is close to or above the Debye temperature of the material. To make results of MD simulations below the Debye temperature more realistic, the quantum correction has to be calculated and factored in. For graphene simulated at $300K$ the quantum correction is $\bar{q} = 0.213$ [22].

## 3.4 LAMMPS

There are different software that implement the MD algorithms, each with its own strengths and drawbacks. In this master thesis the choice of software fell on LAMMPS, acronym of "Large-scale Atomic/Molecular Massively Parallel Simulation". LAMMPS is an open source software solution that can be used to model a wide range of systems, from simple molecules, to large complex structures. Through the support of many different potentials, LAMMPS can be used to study solid state matter, soft matter, mesoscopic materials and more. LAMMPS uses the velocity Verlet algorithm to integrate Newton's equations of motion for systems of particles, where the particles can be clumps of materials, molecules, atoms or electrons. An input script is needed to start a MD simulation in LAMMPS. This script defines all the parameters of the simulation such as units, what potential is to be used, number of steps in the simulation, the size and content of the simulation box, temperature, etc. After the input script is read by LAMMPS the simulation begins, and it keeps running either until it has completed all the time steps, or until one error is met. Typical errors in my experience are "atoms being lost" and/or syntax errors.

The more atoms a MD simulation in LAMMPS has, the more time is needed to complete a simulation. Fortunately LAMMPS has been optimized to be executed in parallel so that the usage of multiple CPU's decreases the total simulation time. By using for example a HPC-cluster (High-Performance Computing), the simulation times can be drastically reduced. The computational time does not only depend on the number of atoms, but also on the algorithms we use to describe the system and on the performance of the machine. It is common practice before performing the production MD simulations, to start off with a benchmarking study to understand how the system scale with more CPU's and what is the optimal choice of the

resources. Those results are then used to argue what amount of computational power it is reasonable to request for a simulation.

## 3.5 Reactive Bond-Order Potentials (REBO)

One of the early struggles of MD was the development of a potential model able to describe the interactions in covalent materials like silicon and carbon. Standard potentials, such as Lennard-Jones (LJ) or embedded atom method (EAM), only describe the interaction between atoms as a function of the distance between them, without considering any directional components in the bond.

One of the first potentials that approached the directionality in the bonds was the Stillinger-Weber (SW) potential, developed to simulate silicon in its solid and liquid state. However in all the family of potentials originating from the SW idea, the connections between the atoms had to be set before to start the simulation, and in general bonds would neither be broken nor created during a simulation. The first potential to incorporate the structural chemistry of covalent bonded systems into empirical potential energy functions [36], was the Tersoff potential, built on work by Abell [37]. The general form of the Tersoff potential is

$$E = \sum_i E_i = \frac{1}{2} \sum_{i \neq j} V_{ij} \tag{3.10}$$

$$V_{ij} = f_c[V_R(R_{ij}) - B_{ij} V_A(R_{ij})] \tag{3.11}$$

where the total energy is $E$, the site energy for site $i$ is given by $E_i$, $V_{ij}$ is the interaction energy between atoms $i$ and $j$, and the distance between these atoms is $R_{ij}$. $f_c$ is a cutoff function to limit the range of the potential. $V_R(R)$ and $V_A(R)$ are pair-additive repulsive and attractive interactions respectively, and their terms are represented by the Morse-type functions [36]

$$V_R = A \exp(-\lambda_1 R_{ij}) \tag{3.12}$$

$$V_A = B \exp(-\lambda_2 R_{ij}) \tag{3.13}$$

where $A$, $B$, $\lambda_1$ and $\lambda_2$ are all positive constants with $\lambda_1 > \lambda_2$. The bonding strength of a pair of atoms in the Tersoff potential is described as a monotonically decreasing function dependent on the number of competing bonds, the strength of these bonds, and the angles between them. $B_{ij}$ has the form

$$B_{ij} = (1 + \beta^n \xi_{ij}^n)^{-1/2n} \tag{3.14}$$

$$\xi_{ij} = \sum_{k \neq i,j} f_c(r_{ik}) g(\theta_{jik}) \exp[\lambda_3^3 (r_{ij} - r_{ik})^3] \tag{3.15}$$

$$g(\theta) = 1 + \frac{c^2}{d^2} - \frac{c^2}{d^2 + (h - \cos\theta)^2} \tag{3.16}$$

The bond angle between bond $ij$ and $ik$ is given by $\theta_{jik}$, while $g(\theta)$ is a global angular function that has to be fit to solid structures of different coordination. $c$, $d$, $\lambda_3$, $\beta$ and $h$ are all positive constants that are fitted to a certain element. In the original paper from 1988 [38], Tersoff had a list of suggested parameters for silicon, and later extended his model for silicone to include germanium, carbon and combinations of them. Donald W. Brenner took inspiration from the Tersoff potential and developed an empirical bond-order expression that described both hydrocarbon molecules and solid-state carbon that he published in 1990 [39]. This was the first generation of the REBO potential where bonds could break and form with changes in hybridization. It was very similar to the Tersoff potential, with the primary difference being the way bond order is handled for hydrocarbon molecules. The total bond order in first generation REBO is

$$\bar{B}_{ij} = \frac{B_{ij} + B_{ji}}{2} + F_{ij}(N_i^t, N_j^t, N_{ij}^{conj} \tag{3.17}$$

where

$$B_{ij} = [1 + \sum G_i(\theta_{jik}) f_c(r_{ik}) e^{\alpha[(r_{ij} - R_{ij}^E) - (r_{ik} - R_{ik}^E)]} + H_{ij}(N_i^H, N_i^C)]^{-\delta} \tag{3.18}$$

Here $N_i^C$ and $N_j^H$ are the total number of carbon and hydrogen atoms bounded to atom $i$, and the total number of neighbours, $N_i^t$, of atom $i$ is $N_i^C + N_j^H$, and $N_{ij}^{conj}$ depends on whether a bond between carbon atoms $i$ and $j$ is part of a conjugated system. $G(\theta)$ is a function of the angle between bonds $i-j$ and $i-k$, and has the same form as in the Tersoff potential [36]. The first generation REBO potential had four main weaknesses:

1. There was one set of parameters that would reproduce structural energies, and another set of parameters that would reproduce force constants. However, because the functional form of the pair potentials was not flexible enough, no set of parameters could be used that would simultaneously reproduce both structural energies and force constants.
2. Zero-Kelvin elastic constants $C_{11}$, $C_{12}$ and $C_{44}$ for diamond were not included in the fitting database and are thus not accurately reproduced by the potential.
3. The values for both the attractive and repulsive forces at zero distance is finite. This can lead to atoms passing through each other without being repulsed in high energy environments.
4. The derivatives of the cutoff function is not realistic and can, in certain structures, lead to spurious minima in the energies.

In 2002, 12 years after the initial paper on REBO, Brenner et al. published a new paper [40] where they presented the second generation REBO potential. Many of the shortcomings of the first generation had been improved upon or fixed. For example, the terms for the attractive and repulsive pairs now had new forms

$$V_R(r) = f_c(r)(1 + Q/r)Ae^{-\alpha r} \tag{3.19}$$

and

$$V_A(r) = f_c(r) \sum_{n=1,3} B_n e^{-\beta_n r} \tag{3.20}$$

where $A$, $Q$, $\alpha$, $B_n$ and $\beta_n$ are fitting parameters. With these new forms the repulsive forces goes to infinity as the distance between the atoms goes to zero, and the attractive term is now flexible enough to simultaneously fit parameters for bond properties that was unfittable in the Morse-type terms. In addition the $B_{ij}$ terms are changed significantly from what they where in the first generation:

$$\bar{b}_{ij} = \tfrac{1}{2}[b_{ij}^{\sigma-\pi} + b_{ji}^{\sigma-\pi}] + b_{ij}^{\pi} \tag{3.21}$$

The values for the functions $b_{ij}^{\sigma-\pi}$ and $b_{ji}^{\sigma-\pi}$ depends on the local coordination and bond angles for atoms $i$ and $j$ respectively. The function $b_{ij}^{\pi}$ is written as a sum of two terms:

$$b_{ij}^{\pi} = \Pi_{ij}^{RC} + b_{ij}^{DH} \tag{3.22}$$

where the value of $\Pi_{ij}^{RC}$ depends on the whether or not a bond between atom $i$ and $j$ has radical character and is part of a conjugated system, while the value of $b_{ij}^{DH}$ is dependent on the dihedral angle for carbon-carbon double bonds [40]. These new terms makes the second order REBO potential also solves the problems with the elastic constants in diamond.

This second generation REBO potential is implemented in LAMMPS. Since this potential is well calibrated to simulate covalent carbon-carbon bonds, as well as larger structures of atoms, it was chosen as the potential to be used to simulate the graphene nano ribbons investigated in this thesis.

## 3.6 My AEMD setup and problems

### 3.6.1 Reproducing results from previous work

Barbarino et al. works study the dependence of the graphene thermal conductivity on the graphene sample size, [8, 22]. Their work is a relevant starting point for my masters thesis. From her thesis [22] I have chosen some data points to reproduce since her work has been performed with the AEMD technique coupled with the REBO potential. My prior experience with MD simulations was the computational study of Argon using the Lennard-Jones potential; I have fully expected to encounter a learning curve and that I would do some mistakes on the way. Knowing this, and that MD simulations often require a non-insignificant time to complete, I chose to reproduce the data from her smallest graphene sample, since this should give me the simulations that would run the fastest. The first simulations I have performed to reproduce her data took 2-3 days to be completed. However, I have learned how to optimize the code, utilizing the HPC server better and getting more familiar with the methods I used. My experience shortened further the completion time of similar cases down to 3 hours per simulation.

Apart from the obvious challenges of comprehending her work and supplementing it with journals detailing the methods used, the biggest challenge was to decide how to deal with descriptions sometimes not being detailed enough, leading to multiple procedures having to be considered. For instance, when calculating the thermal conductivity from the thermal diffusivity, part of the calculation involves dividing on the volume of the simulated sample, 3.9. Since the thickness of the simulated graphene was not defined, sensible choices could be made of values ranging from 1Å and 3.35Å, something that would drastically change the results. Also, it was not clear if the length of the graphene were given as the initialized length, or as the length it had at the start of the nve simulation where $\Delta T(t)$ was recorded.

The way I resolved these questions was by brute force. First I calculated the distance from the "center of atom" on one side to the "center of atom" on the opposing side. This is one way the length could be defined. Lets call this method A. Another way would be to take length in method A but add either the van der Whaal radius of carbon to each side, lets call this method B, or add one bond lenght, method C. Looking at figure 3.2 method A is represented as the blue line and method C is represented as the blue + green lines inside one box. Option B is not in the figure, it would be the blue line plus 2× van der Whaal radius of carbon.

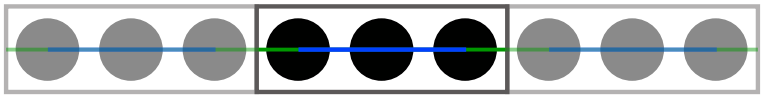

**Figure 3.2:** In this figure the length is measured as a "center of outer atom" to "center of outer atom on opposing side" represented by the blue line. The green lines represent "half the bond length" and by adding them we now have the length of the repeating structure.

When deciding how to measure the thickness of the graphene plane, method A would not work since it would just be zero. Method B and C could work and would be 1.41Å or 2× van der Whaal radius of carbon. However, it was possible that Barbarino had just set thickness to 1Å to get the units of the calculation correct, or that she used the length between graphene layers in graphite, 3.35Å.

In total this adds up to 27 different ways to define the volume. By requiring the same methods to be made in both directions in the graphene plane, this was cut down to 9 different options. So I calculated the thermal conductivity $\bar{k}$ 18 times, 9 times for the initialized dimensions of the graphene, and 9 more times for the dimensions the graphene had at the start of the nve simulation where $\Delta T(t)$ was recorded. The best fit with the results Barbarino reported, were achieved when measuring the size of the graphene plane by using method C, while using 1 as the planes thickness. And the data giving the best fits was the positions the atoms had at the start of the nve simulation where $\Delta T(t)$ was measured.

Another thing that was not clear to me was how the periodic boundary conditions (PBC) had been used in the work I wanted to reproduce. Since the work explores the length dependency of the thermal conduction, it would make sense if

the length dimension was fixed. If not, the simulation would represent an infinite plane of graphene in all directions. I have recorded the temperature profile while simulating each option. By plotting the profiles and then comparing them to the profile presented in Barbarino's work, [22], it was clear that the PBC were used for monitoring the temperature profile. To be sure, I also ran full simulations with fixed x-dimension, but the results from those simulations where not anywhere close to the results reported.

Having settled on how I think Barbarino had done her simulations, I performed the final simulations to reproduce the data five times. Each run had slight differences in the number of MD-steps used in the different parts of the equilibration of the graphene sample. The random number seeds were also changed in the independent simulations. The average of the five runs were calculated and the results agree well with the one presented in Barbarino's work4.

### 3.6.2 Protocol to simulate hydrogen-free (pristine) GNRs with AEMD

My implementation of the AEMD method ended in an input script that could be divided in seven steps:

1. Initialization: In this part all parameters annd simulation box are set, the potential and the initial data file of the GNR are read.
2. NPT equilibration: The sample is equilibrated with a Nose-Hover thermostat and barostat set to $T = 300K$ and $P = 1bar$. During this step the volume of the simulation box can change as the system reaches equilibrium.
3. NVT equilibration: Nose-Hover thermostat is used to keep the temperature at $300K$ while the system is kept at a fixed volume to allow the system to reach the correspondent pressure.
4. Definition of two separate regions: The left and right regions are defined separately as in figure 3.1, and different computes are set to calculate the temperatures in them.
5. Thermal equilibration of the "left" region. The right region is not integrated, while the velocity rescaling is applied to the left region in order to set instantaneously $T_{left} = 400K$. A Nose-Hover thermostat further equilibrate the temperature of the left region at $400K$ for a certain number of MD steps.
6. Thermal equilibration of the "right" region. The left region is now kept at $T_{left} = 400K$ and not integrated, while the velocity rescaling is applied to the right region in order to set instantaneously $T_{right} = 200K$. A Nose-Hover thermostat further equilibrate the temperature of the right region at $200K$ for a certain number of MD steps. Up to this stage left and right regions are separated.
7. NVE simulation for the whole sample: both regions are put in contact and free to interact. The thermal equilibration starts and $\Delta T(t)$ is recorded during this part of the simulation. When $\Delta T$ reaches a value close to 0, the AEMD simulation is completed and the post processing stage starts.

While reproducing results from Barbarino, these steps worked well since the

PBC meant that the simulated graphene sample was in a sense "infinite", so when oscillations in the graphene pushed a carbon atom out of the simulation box on one side, it just reappeared on the other side. By setting the dimensions of the simulation box correctly compared to the size of the graphene sample, the carbon bonds stayed intact across the boundary and these jumps had no real impact on the results of the simulation.

However, when doing simulations of hydrogen-free nano ribbons of graphene, the dimensions of the simulation box needs to be set a lot bigger than the size of the graphene sample in the y and z direction ($x$-direction being the direction to which the heat gradient is applied), else the ribbon will act as a plane instead of a ribbon. This makes step 2 of the simulation challenging 3.6.2, since when the simulation box changes during the NPT run, it tends to become smaller than the initialized box where the ribbon is straight, thus leading to the ribbon curling up and the reactive edges of the ribbon binding to other parts of the ribbon as seen in figure 3.3.

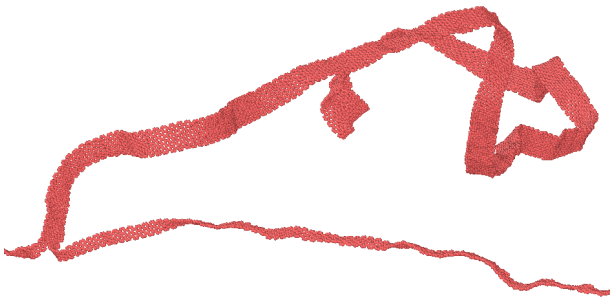

**Figure 3.3:** Hydrogen-free GNR that curls up and reacts with itself during the equilibration steps of AEMD simulation.

To overcome this challenge I chose to build my GNR and initial simulation box just as I had done when reproducing results. This meant that for steps 1 to 3 in the simulation, my GNR would be simulated as an infinite sheet of graphene. Then, in step 4, I would rescale the simulation box in the $y$ and $z$ directions, such that there would be a lot of empty room between my sample and the simulation box in the $yz$-plane. I would not do any scaling in the $x$ direction since the AEMD method calls for PBC [6][7]. However, there was still one problem; the carbon atoms that jump across the boundaries. As explained earlier, this is not a problem when simulating a plane of graphene, but it is a problem when simulating ribbons. Figure 3.4 show some typical edge defects that the ribbons ended up with following this method of running the first few steps as a simulation of a "plane of graphene". The effect of these defects is that the thermal conductivity of the ribbon goes down, and since the defects seem a bit random they affect the different size ribbons differently, leading to a lot of noise in the results of the calculated thermal conductivity.

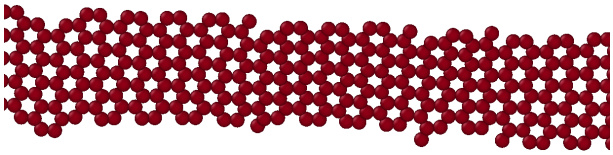

**Figure 3.4:** Typical edge defects on the GNR after being equilibrated as a sheet of graphene. These defects can scatter phonons.

By changing the length of the time steps from $1fs$ to $0.1fs$ during step 2 and 3 of the simulations, while also letting these steps run for a total of only $200ps$, the defects went away. I inspected each ribbon in OVITO (software) from start to end, to verify that they had no defects. When I found defects, I changed to equilibration to a smaller value and also changed the random number seeds and ran it again until I got defect free ribbons. The lowest I had to go on equilibration time to achieve this was $100ps$.

For graphene nano ribbons built in the zigzag orientation (3.7), ZGNR, this method only works for the ribbons consisting of an even-number of strips, since the odd-numbered configurations does not represent a graphene plane when simulated with PBC. To simulate the odd-numbered configurations I saved the configuration of the even-numbered systems after step 3 in their simulation was complete. Then I manipulated those data files by removing one strip from the edge of the ribbon. The manipulated data files would then be the initial configurations read into the simulations of the ZGNR's with an odd-number of strips, and the AEMD run for these ribbons would ignore step 2 and 3 and instead go straight from step 1 to step 4 in the MD simulation (3.6.2). These simulations got double the time to equilibrate in step 5 and 6 compared to the ZGNR's with an even number of strips.

### 3.6.3 Measuring the size of a GNR

As mentioned in the section 3.6.1, when using the AEMD method, the calculations of the volume of the simulated sample has a big impact on the resulting thermal conduction $\bar{k}$. Since this work is exploring what happens as the width of the GNR's gets smaller and smaller, the choices made will have a higher and higher impact on the calculated $\bar{k}$, until we are at the mono-atomic carbon chain. I will therefore go trough my choices of how I have measured my GNR's in each direction.

#### $x$-direction

For the $x$ direction I decided the most sensible measurement is to measure it from the center of the first atom to the center of the last atom, then adding the length of one bond. This is done because the ribbon is simulated with PBC so it is in sense a part of an infinite ribbon, and the measurement would not properly reflect this if one bond length was not added. Since the $x$-length is on the order of $2 * 10^4$Å this choice has minimal, if any, impact on the result. However, something that has

a great impact is at what point in the simulation the length is measured. In figure 3.5 the starting configuration of 1 strip in the armchair configuration is shown, and it is obvious that the length in of the sample is identical to the length of the simulation box.

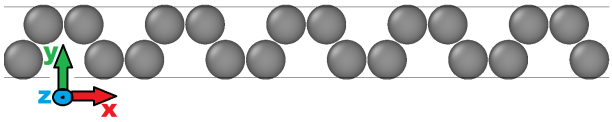


**Figure 3.5:** This is the starting configuration of the 1 strip in the armchair configuration. The lines represent the initialized simulation box. Because of the regularity, the dimensions of this shape is fairly simple to describe precisely.

However, after the sample has had time to equilibrate, all the bonds have slightly different lengths, and for the 1 strip case the structure of the sample has also broken down. In addition to this the simulation box have changed its size and the ribbon is now coiled up in a more complex pattern, part of which can be seen in figure 3.6. Finding the length of this sample is no longer an easy task. The 1 strip armchair case is of course an extreme example since the structure breaks down and it forms a mono-atomic chain, but it is also true for the 2 to 10 strip GNR's that they change their orientations and that they will no longer just be straight lines after equilibration.

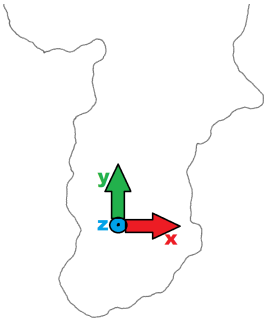


**Figure 3.6:** This is a small part of the final configuration of the 1 strip armchair configuration after the structure has broken down. The dimensions of this shape is no longer fairly simple to calculate or describe precisely. The whole figure can be found in the appendix A.4.

My solution to this problem was to use clever numbering of the atoms in the initial configuration of each GNR, save a data file with the initial configuration, and save another file with the configuration at the start of the 7th step of the simulation (3.6.2). Assuming that atoms belonging to the center strip of the GNR still belonging to the same strip after the equilibration, I now used the atom numbers to isolate a "dimer line" of atoms close to the center of the ribbons. All atoms on the same dimer line shares $y$-coordinate in the starting configuration as shown in figure 3.7.

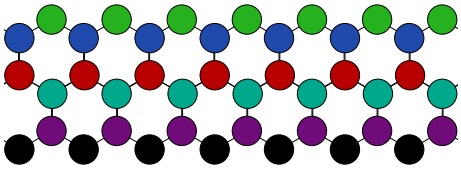

**Figure 3.7:** Each color represent a "dimer line" through the graphene sample. In its initial configuration all atoms on a dimer line can be identified by having the same $y$-coordinate as the rest of the atoms on the same dimer line. When the GNR has equilibrated the atoms on a dimer line will no longer share $y$-coordinate, but their ID number will still be the same.

Lastly I wrote a python code that would calculate the vector distance between the atoms along the dimer line, and then give the sum of these distances as an output. With this code I could get a sensible length of the 1 strip armchair shown in figure 3.6 and I could also get accurate lengths of the GNR's, no matter how they moved through the simulation box. What I do not cover with this method is how rotations and twists of the GNR affects the lengths, but it seems clear that a twisted GNR in general will have a larger surface area and thus $x$, $y$ or both will get higher values. The result of this is that the thermal diffusivity will be divided on a larger volume when the thermal conduction is calculated, leading to a lower thermal conductivity than the non-twisted case, an observation that agrees with other work [41].

### $y$-direction

For measurement of the $y$-direction I choose to use the distance between center-of-atom on one side, to the center-of-atom on the opposing side, and then add a bond length, a method I called method C in section 3.6. This method was only used for the case of 2 to 10 strip GNR's. Since the 1 strip case is not a GNR, it has no rigidity and looses its initialized structure, becoming a mono-atomic chain where the $y$ and the $z$ directions are indistinguishable. This must be reflected in the same choice of measurement being chosen for both directions.

### $z$-direction

The measurement of the $z$ direction and the $y$-direction, in the one strip case, was set to a value of 3.35Å since this is the interlayer distance in graphite. For the GNR cases (2-10 strips), the $z$-direction was also set to 3.35Å. This was done to be in line with the suggestion of a standard choice of thickness when calculating thermal conductivity in single-layer materials presented in [42]. This will lead to my calculations of thermal conductivity having lower values than in some other papers like for example [8]. However, since I have seen at least 4 different thicknesses used in the journals I have read, I choose to follow the standardisation in [42] to try to be part of the solution.

## 3.7 Building the graphene

Thermal transport in graphene has the exotic feature that it is dependent on both the length [22] and on the width [26] of the material. A consequence of this fact is that the length of the graphene nano ribbon's, GNR's, simulated in this work should be chosen with some care. This is because the length of the simulated GNR's will change as they are heated up in the simulation, and in case there are variations in how much the different ribbons expand, the effect this has on the thermal diffusivity should be minimized. At the same time, the computational cost of the simulations has to be kept in mind. In [22] it is found that the increase in thermal diffusivity as the samples length increases, is flattening out over the span from $1\mu m$ to $100\mu m$. Therefore the simulated GNR's should be as long as possible. However this quickly requires too much computational costs and time, something that is especially important since I expect to do mistakes as I learn, and thus will have to rerun the simulations multiple times. Therefore a length of $2\mu m$ was chosen.

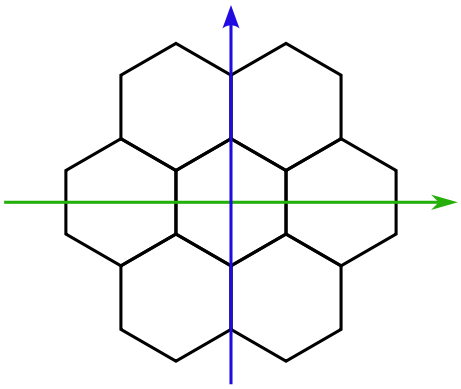

**Figure 3.8:** The two axis of symmetry in graphene shown by a blue and a green arrow. The green arrow points in the "armchair" direction while the blue arrow points in the "zigzag" direction.

To probe what happens as a GNR's width decreases down to a quasi one dimensional string of carbon atoms, the ribbons need to be divided into similar parts that can be removed one by one. As can be seen in figure 3.8, graphene has two axis of symmetry. When building a GNR with length in the armchair direction, the task of finding similar parts that can be removed one by one is easy. In this work these parts will be referred to as "strips" and in figure 3.9 the different strips are show in different colors. Each strip is built up by two dimer lines (3.7). For strips building ribbons in the armchair orientation, all the strips can be identical and stacked on top of each other until the desired width is reached. In this work the widths of 1 to 10 strips will be investigated. In the 1 strip case its important to notice that this is no longer a graphene sample since there are no completed hexagonal structures present. For the 2 to 10 strip cases the strips form hydrogen free graphene nano ribbons, GNR's, either in the armchair orientation, AGNR, or

the zigzag orientation, ZGNR.

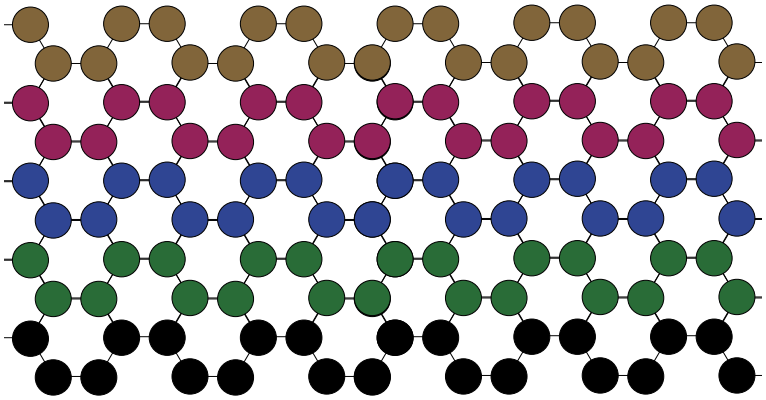

**Figure 3.9:** A section of a 5 strip AGNR (GNR built in the armchair direction). The different strips have different colors so that they are easy to see. Every strip has the exact same structure and are stacked on top of each other to make up the ribbon.

When it comes to the other direction of symmetry, the zigzag direction, a slightly different approach has to be used. This is because every other strip is mirrored along the width axis. This means that odd numbered strips look the same, the even numbered strips looks the same, but the odd and even strips are mirrored. How this looks can be seen in figure 3.10.

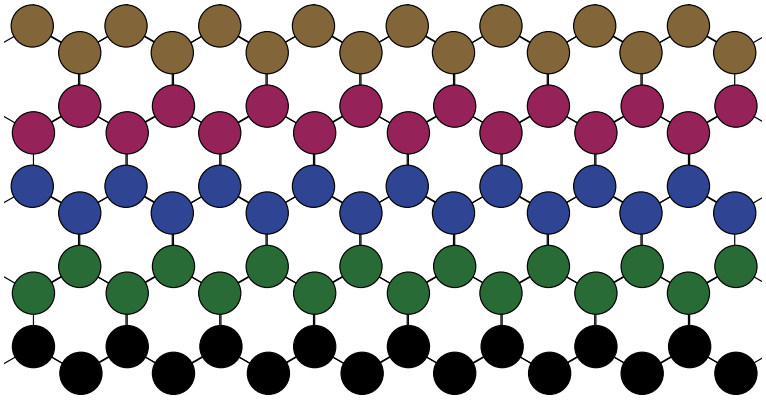

**Figure 3.10:** A section of a 5 strip ZGNR (GNR built in the zigzag direction). The different strips have different colors so that they are easy to see. Here the black, blue and brown strips are the exact same structure, and the green and red strips are the exact same structure. The two structures are mirrored version of each other.

# Chapter 4

# Results and discussion

In the following sections, the most important findings and results will be presented. Because of other previous works, I have decided to investigate hydrogen-free graphene nanoribbons. For a 1 chain-strip of carbon atoms, I observe collapse and anomalous behavior as expected. That configuration is indeed an extreme one where the system loose the graphene character. I have not presented the 1 strip cases in this chapter but in the appendix. However, I am referring here to the 1-strip case to study the bond length variation.

## 4.1 AEMD implementation tests

I have spent the initial time of my master thesis to implement the AEMD method described in section 3. Among the numerous tests I have done, I am discussing and comparing here the temperature profiles and the fitting procedure of the AMED implementation on my system. As explained in more detail in Chapter 3, the AEMD procedure implies the definition of two separate regions of equal volume, regions 1 and 2. Those two regions are individually and separately equilibrated at two different Temperatures, $T_1$ and $T_2$, such that $T_1 > T_2$. I refer to $t = 0ps$ as the time at which the two regions are separated and fully equilibrated at two different temperatures. This initial stage determines a gradient of temperature $\Delta T = T_1 - T_2$ with respect to the $x$-dimension. In a second stage, the two separate regions are set in contact, and I have monitored the temperature profile at different time snapshots. The evolution of the difference in temperature, $\Delta T = T_1 - T_2$, between the two regions is also observed. From the fitting of time evolution of the temperature gradient, the diffusivity is extracted, and, the thermal conductivity $k$ is calculated from the diffusivity as explained in Section 3.

### 4.1.1 Temperature profile

In figure 4.1 the temperature profile from my implementation of the AEMD method is presented at three different MD time snapshots for the case of a graphene sample with dimension $(500 \times 2.4 \times 0.3)nm$ containing 48000 atoms during an NVE simulation.

I have monitored the temperature profile during the temperature equilibration of the two regions set in contact, i.e. from time $t = 0ps$ to $t = 500ps$. Figure 4.1 shows the Temperature (K) for three different time steps along the length of the sample, i.e. x (nm), to which the gradient of Temperature $\Delta T$ is applied. The timestep $0ps$, red line in the graph, refers to the temperature profile at the time in which the two regions at different temperatures, $T_1 = 400K$ and $T_2 = 200K$, are put in contact. The red line appears close to a step function. After $20ps$, the blue line in the figure, the temperature profile assumes a sinusoidal shape with an amplitude. The sinusoidal shape decreases its amplitude over time until the temperature in both regions reaches the same value, i.e. $300K$. This plot agrees well with similar plots found in [6] and [7] guaranteeing the correct implementation of the AEMD protocol.

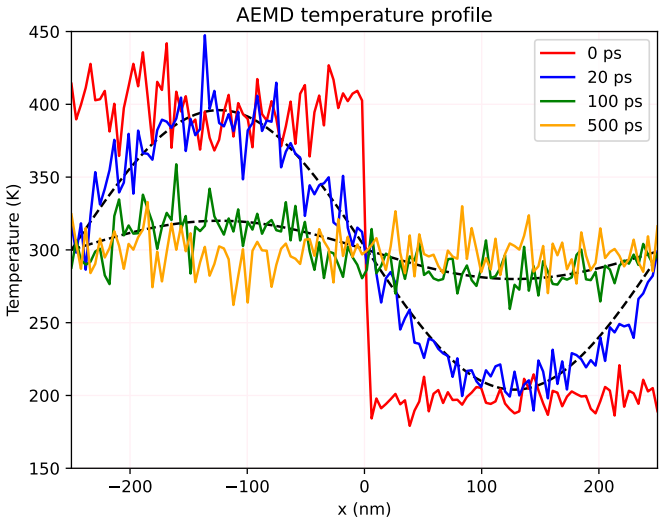


**Figure 4.1:** Temperature profiles during an AEMD simulation at the beginning of the NVE equilibration (red), after 20$ps$ (blue), 100$ps$ (green), and finally 500$ps$ (yellow). The dashed lines represent sine fits of the temperature profile at 20$ps$ and 100$ps$.

### 4.1.2 Fitting temperature equilibration

As already explained, according to AEMD, the thermal diffusivity is obtained by the fit of the $\Delta T = T_1 - T_2$ data coming from the NVE simulation of the system made of the two regions at Temperature $T_1$ and $T_2$, that are now in contact. Figure 4.2 shows the plot relative to my 9 strips ribbon in the armchair orientation. The fitted function fits the plotted data well.

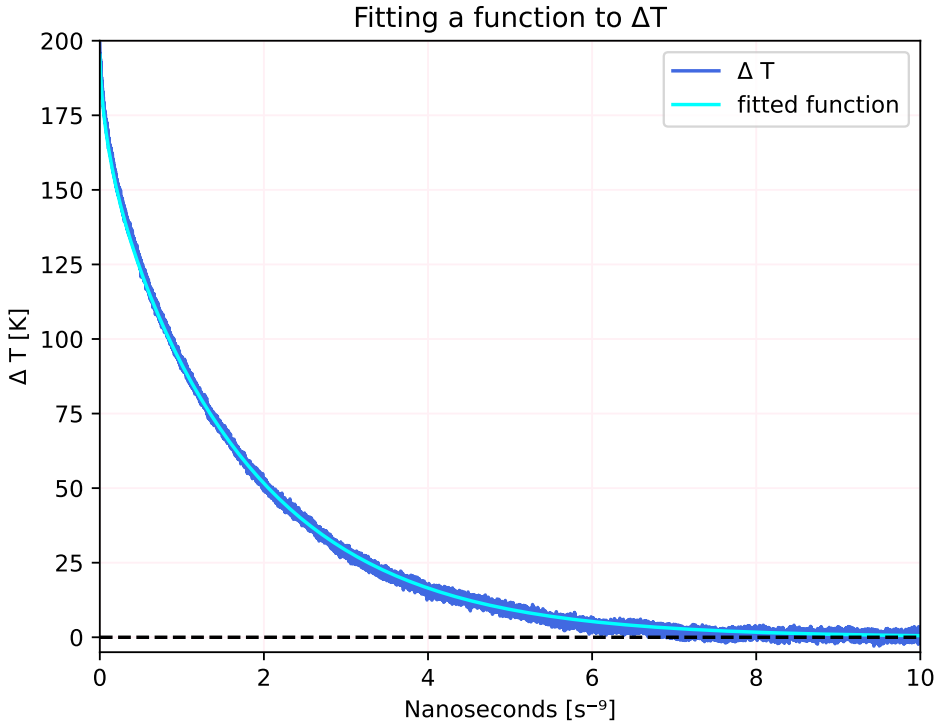


**Figure 4.2:** $\Delta T$ time evolution for the armchair 9 strips AEMD simulation, blue line, and fit-function, cyan line, that was used to find a value for the thermal diffusivity. The dashed black line shows the reference $\Delta T = 0$

In figure 4.3 there are two plots of data from a simulation of a 2 strips ribbon in the armchair orientation. The top plot shows the calculated thermal diffusivity $k$ as a function of the time simulated, while the bottom plot shows the evolution of $\Delta T$ as a function of time simulated. Together these plots shows that in the case of this specific AEMD simulation, nothing is gained from running the simulation after the point where $\Delta T = 0$. It also shows that, in this particular simulation, the $k$ calculated after $280ps$, with $\Delta T = 7.4K$, is 98% of the full $k$ value that is reached after a $600ps$ long simulation, with $\Delta T = 0K$. If this relation between simulated time and calculated $k$ holds for all the simulations, it means that the computational cost of the simulations can be reduced by sacrificing 2% in the precision. To conclude, for very time consuming simulations, I have confidently considered to calculate $k$ where the $\Delta T$ has reached a value around $5K$.

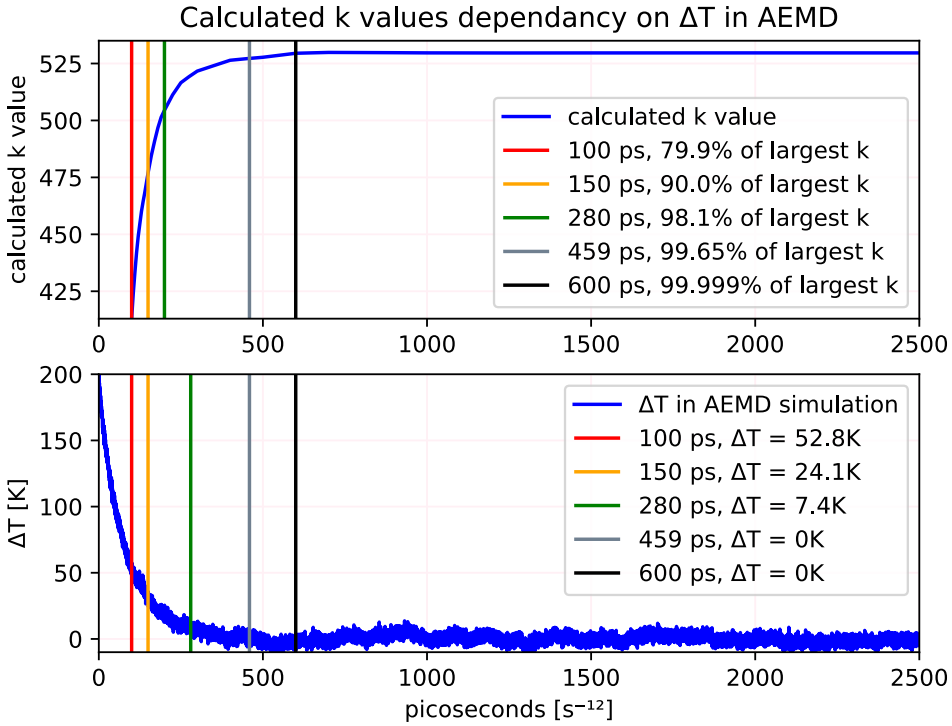


**Figure 4.3:** Data comes from an AEMD simulation of a 2 strips armchair ribbon . Top plot shows the $k$ value as a function of simulation time; Bottom plot shows the corresponding temperature difference between the hot and cold region against the simulated time. The "largest $k$" mentioned in the legend, is the value of $k$ when it stops changing. In the plot this is where the blue line becomes just a horizontal line.

## 4.2 Potential benchmarking

In this section, I am presenting the preliminary study I have done to understand the optimal requests of CPU's and nodes while using the REBO potential. As already stated, I have used the HPC facilities at the physics department in NTNU to carry out my simulations. There is a SLURM scheduler in the HPC system, and to start my simulation I have used a standard submission script where I could request the necessary computational resources, as number of nodes and CPU's. In the first part of this section, I present the performance of the simulation in term of nanoseconds per day for different combinations of tasks per node (ntask) and CPU's per task (omp). Furthermore, the strong scaling and efficiency of the potential per number of CPU's, and per node, are also presented.

### 4.2.1 Performance

Figure 4.4 shows the performance for the same initial system simulated with different settings in the SLURM job submission script. I used the same sample settings as I would to perform my work, and ran a NPT simulation simulating a $2\mu m$ long 8 strip AGNR, consisting of a total of 151680 atoms, for 2000 MD-steps with $1fs$ time units. The plot shows that the fastest way to complete this particular simulation is achieved by using the SLURM job settings of "ntask = 40" and "CPU's per task = 1", with the omp flag enabled in LAMMPS[1].

[1]Too see the impact of omp flag vs no omp flag see appendix A.6

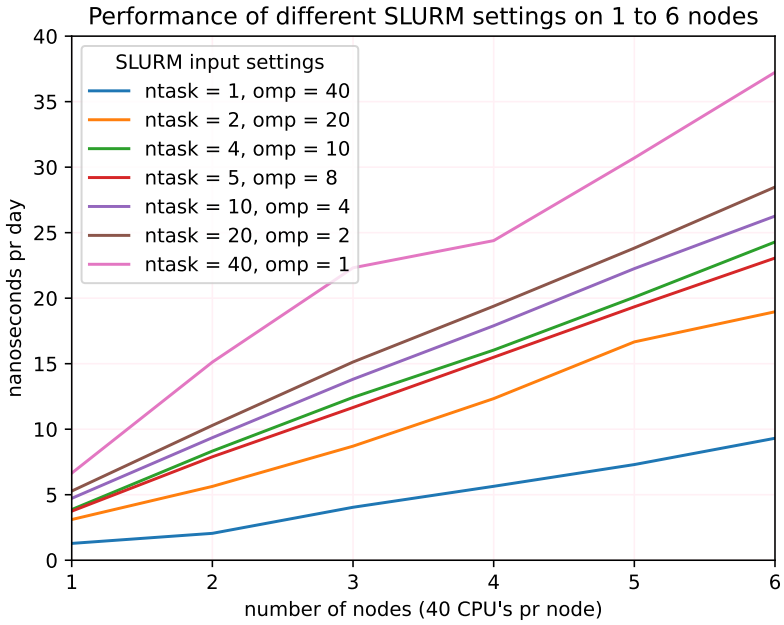


**Figure 4.4:** Nanoseconds per day against number of nodes for different combination of Ntask (number of tasks per node) and omp (number of CPU's per task). All runs were done with the omp flag enabled in LAMMPS, and the number of omp set in SLURM matched the number that was also set in LAMMPS.

### 4.2.2 Strong scaling and efficiency

The strong scaling results were obtained by running a NPT simulation of a $2\mu m$ long 8 strips AGNR for 2000 MD-steps, totaling $2ps$, on the "norma2" partition of the physics departments HPC server. This partition consists of 6 nodes, each with two 20-core CPU's with Hyper-Threading. However, initial testing showed that use of Hyper-Threading when simulating with the REBO potential[2] made the simulations run slower, therefore, I did not enable Hyper-Threading when running simulations, and it was not used for the strong scaling benchmark simulations either.
The strong scaling graphs are based on the calculation of the speedup factor for different number of CPU's or nodes

$$Speedup = t(1)/t(N), \tag{4.1}$$

where $t(1)$ is the time it takes to run the task on 1 CPU and $t(N)$ is the time it takes to run the task on $N$-CPU's.

The left plot of figure 4.5 shows the speedup against the CPU's number on a single node. Up to 10 CPU's the real speedup, blue symbols, coincides with

[2] See appendix A.5

the ideal speedup, red dashed line. After this limit, the real speedup is reduced with respect to the ideal case, with a final speedup of 26 compared to the ideal speedup of 40. The right plot of figure 4.5 shows the speedup against the number of nodes. From the first to the third node the speedup is linear, then it deviates for three to four nodes, to appear again linear for four nodes. The final speedup is 120 compared to the ideal speedup of 240.

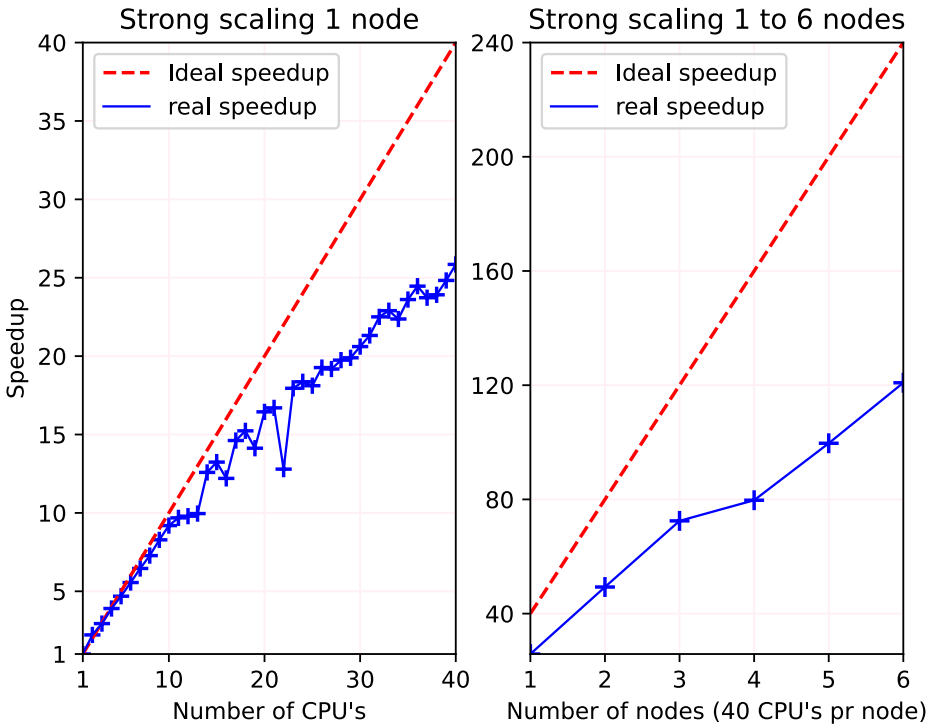


**Figure 4.5:** In the left plot, strong scaling against CPU's on a single node. In the right plot, strong scaling for 1 to 6 nodes. Since the nodes have 40 CPU's each, the plots cover the strong scaling from 1 to 240 CPU's. The red dashed lines represent the ideal speedup, while the blue lines represent the real speedup.

Figure 4.6 shows the efficiency corresponding to the strong scaling graphs in figure 4.5. The left plot shows the efficiency against the CPU's on a single node, while the right plot shows the efficiency against the number of nodes. Between 1 and 3 nodes the efficiency stays close to 0.6 before it drops down to 0.5 for four to six nodes. This shows that going from three to six nodes, thus doubling the computational power, only leads to an increase of $\frac{2}{3}$. Depending on the demand and cost of the added computational power, it could therefore be better to run the job on 3 nodes only.

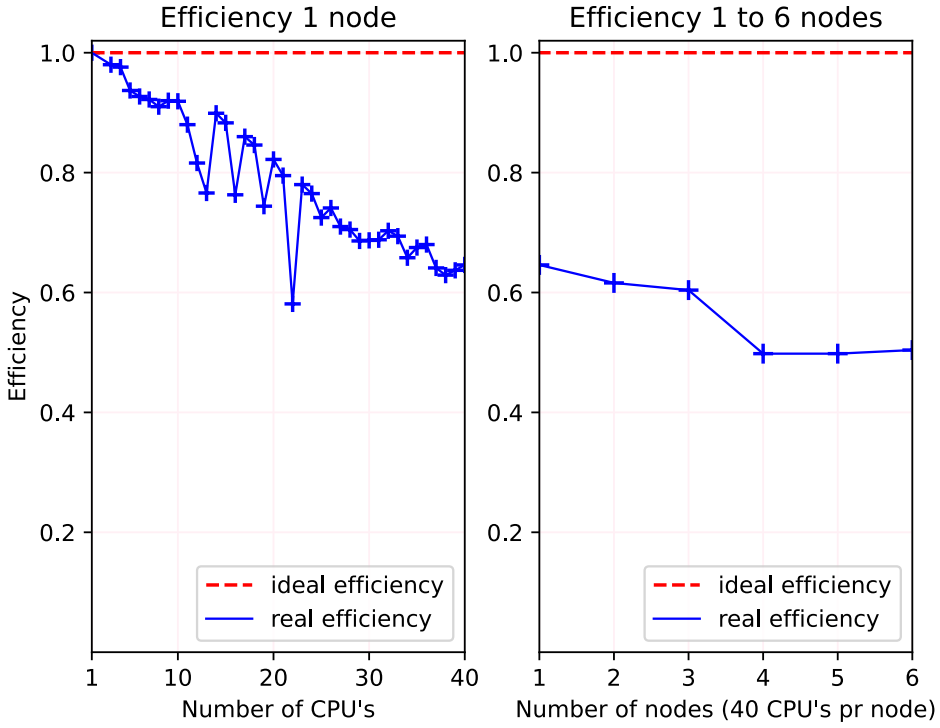


**Figure 4.6:** These plots shows the efficiency of the simulations used to create the strong scaling plot in figure 4.5. The left plot shows the efficiency against number of CPU's used on a single node, while the right hand plot shows the efficiency against nodes' number. Each node has 40 CPU's so in total the plots show the efficiency running the same simulation on 1 to 240 CPU's.

## 4.3 Thermal conductivity of Graphene by AEMD

In this section I am explaining the main thesis results. In the first subsection I am showing how my simulation settings have successfully reproduced the data from previous works [8, 22]. The second subsection is dedicated to the calculation of thermal conductivity for different graphene nanoribbons samples.

### 4.3.1 Reproduction of the previous literature

The reference literature for my thesis were the work of Barabarino and others [8, 22]. The results and conclusion of their investigations have been presented in Chapter 2. Figure 4.7 has been extracted from the paper [8], and it presents their thermal conductivity prediction for different length of the sample. The length of the sample is also the direction of the applied gradient by AEMD approach. In particular, I have considered the thermal conductivity prediction for a $830nm$ long and $0.7nm$ wide Graphene sample. According to the graph, $k = 547.55\ WK^{-1}m^{-1}$ [22]. I have performed five distinct simulations for an identical starting sample, and, I have obtained a thermal conductivity $k = 550.727\ WK^{-1}m^{-1}$ with a standard deviation of 12.527. This result is in very good agreement with Barbariano's result, and gives good reason to believe that my implementation of the AEMD method has been done correctly.

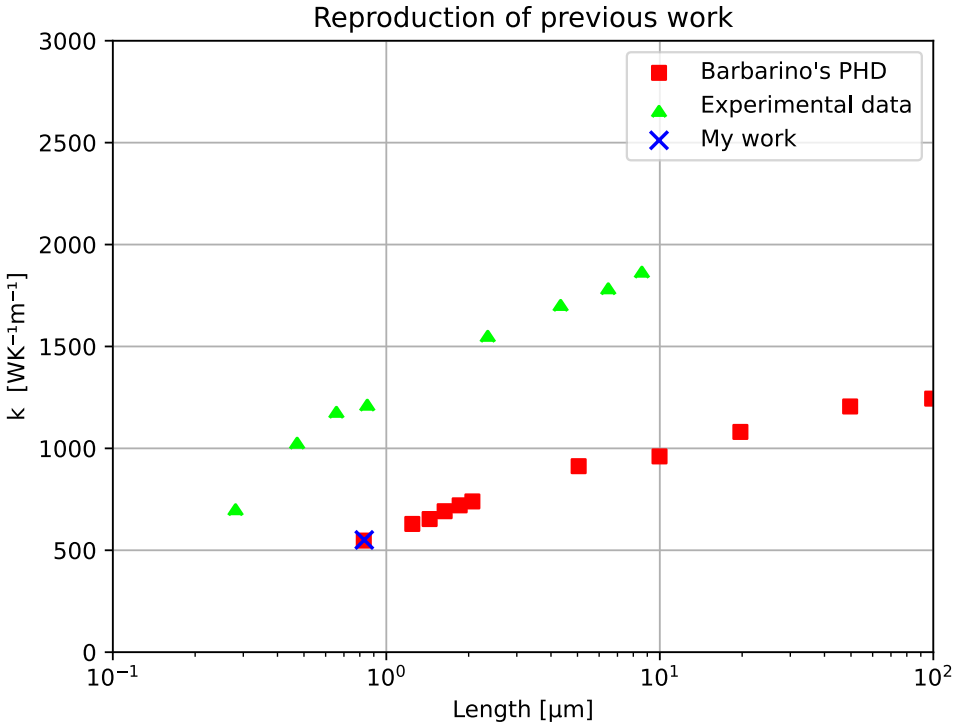


**Figure 4.7:** Modification of Figure 4.6 in [22]. Respect to the original data, I have added my simulation point, blue cross. The red squares and the green triangles are the points from the original Barbarino's figure.

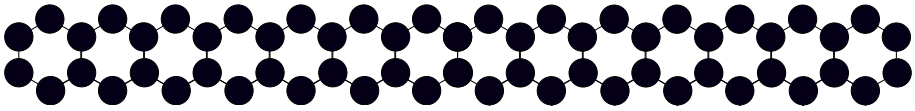

**Figure 4.8:** A single layer of the honeycomb structure of graphene. In this work this specific one is called a 2 strip zigzag graphene nano ribbon, or 2 strip ZGNR for short.

## 4.4 Thermal conductivity of quasi-1D system

In this section I am presenting my simulation study to investigate the dimensionality effect on the thermal conductivity. I have calculated the thermal conductivity for a 2D Graphene sample and I have stripped out "a line of carbon atoms" sequentially reducing the width of the sample to reach the limit configuration that contained only one hexagonal honeycomb lattice series as in figure 4.8. The starting strip for the armchair ribbons contains 18960 atoms and has a dimension of $2016nm \times 0.3nm$, while the starting strip for the zigzag ribbons contains 16320 atoms and has a dimension of $2004nm \times 0.2nm$. There are 9 ribbons for each of the armchair and zigzag configurations, and they consist of 2 to 10 strips. The data discussed in this section have been obtained post-processing the data from AEMD simulations at $T = 300K$ as discussed in section 2 and 3.

### 4.4.1 From 2D to 1D

I have decided to simulate hydrogen-free graphene ribbon, since experimental and theoretical calculations [24, 43] provided confirmation the non-functionalized edges can exist. I have noticed that for the limit sample consisting of 1 strip, the armchair and zigzag orientation of the carbon atoms breaks down. This happens because there is little rigidity in a single strip, so as the atoms vibrate and the bonds stretch or contract, the bonds reorient themselves until they end up on opposite sides of the carbon atom, forming a long chain of carbon atoms. This long chain has a lot higher values for $k$ than the 2 strip ribbons, leading to plots of $k$ not showing other features than the difference between 1 and 2 strips as can be seen in figure A.1 in the appendix. The following plots of $k$ values presented in this section will therefore not include the 1 strip results.

In figure 4.9 there is a plot of $k$ values for $2\mu m$ long hydrogen-free graphene ribbons built up by 2 to 10 strips. The ribbons that are built in the armchair configuration has carbon-carbon bonds that are parallel to the direction of the heatflow, while the ribbons built in the zigzag configuration has no carbon-carbon bonds that are parallell to the heatflow.

Figure 4.9 shows the comparison of the thermal conductivity for Armchair Graphene Nano Ribbons (A-GNR)and Zizag Graphene Nano Ribbons (Z-GNR) configurations against the number of strips. The calculation have been performed with the AEMD approach as explained in Section 2. The graph clearly shows that the thermal conductivity of Z-GNR is higher for than the A-GNR configurations,

the same conclusion was reached by another Non equilibrium MD study [43], that applied NEMD with the Tersoff potential. However, the study is referring to much wider samples, and this could maybe justify the absolute value of their TC predictions higher then mine, despite the fact the order of magnitude is consistent. Furthermore, the order of magnitude of $k$ is also in well agreement with the experimental data presented in figure 2.4, and in papers [24, 26] that are discussed in section 2.

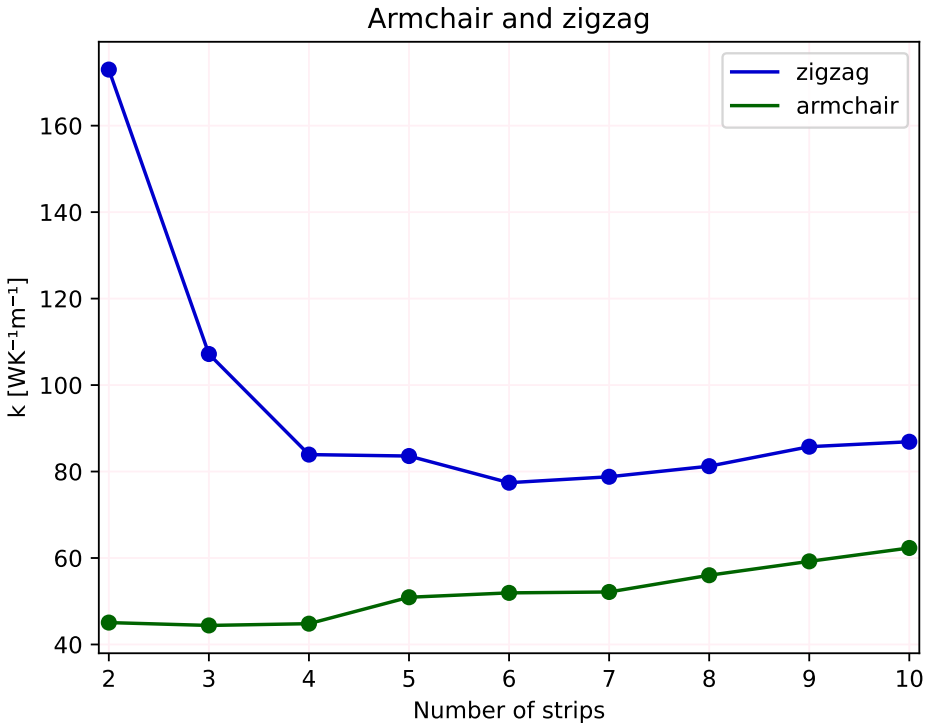


**Figure 4.9:** The decrease in $k$ when strips are removed in the armchair configuration, is a lot smaller than the increase in $k$ in the zigzag direction.

In figure 4.10 the average length of bonds in the direction of heat flow is plotted for the different ribbons. These bond lengths have been calculated by the distances between atoms in a strip close to the center of a ribbon, and therefore does not tell us anything about the bond length in the other directions. As strips are removed from the ribbons, the bond lengths starts to increase. For the 1 strip case the zigzag and armchair structure of the strips collapses, and they end up as long strings of carbon that coil around in the simulation box. At this point there is no difference between zigzag and armchair, something that is underlined by the bond lengths becoming identical.

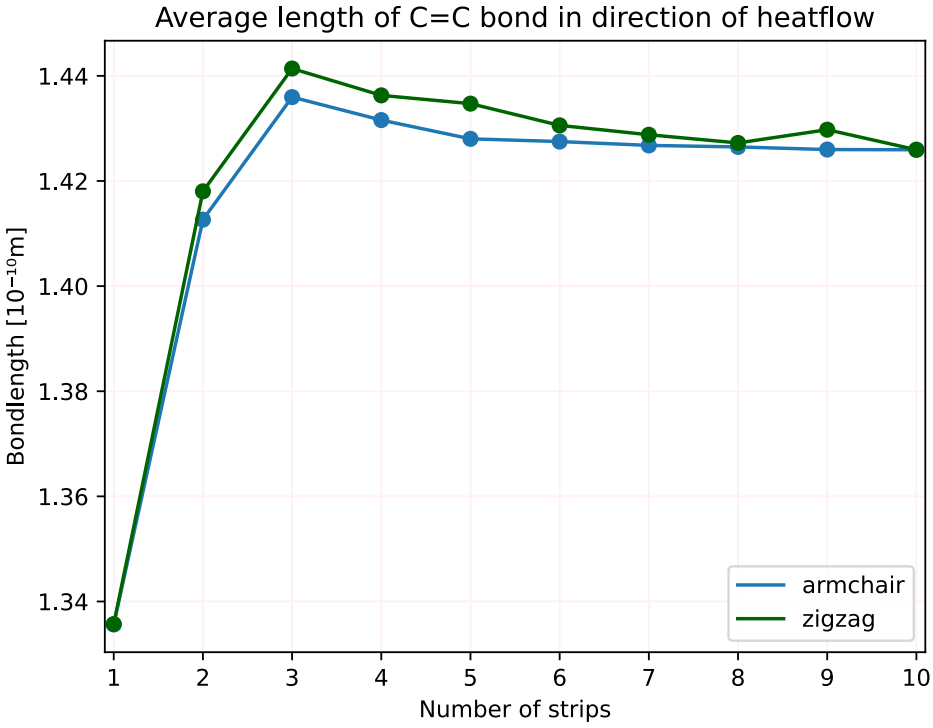


**Figure 4.10:** Bond length at different equilibrated zigzag and armchair edge-configurations containing different number of strips.

This change in bond length leads to the overall length of the samples, changing, from the initial configuration of 2004.14$nm$ for the zigzag and 2016.4$nm$ for the armchair before the simulations begin, to some higher value that has to be calculated. The final calculated lengths of the samples are presented in figure 4.11.

The largest change in length going from 10 strips to 2 strips happens for the armchair orientation. This is because the armchair orientation has 18960 atoms per strip while the zigzag orientation only has 16320 atoms per strip, so when the two different orientations undergo an identical growth in bond length, the armchair orientation changes the most.

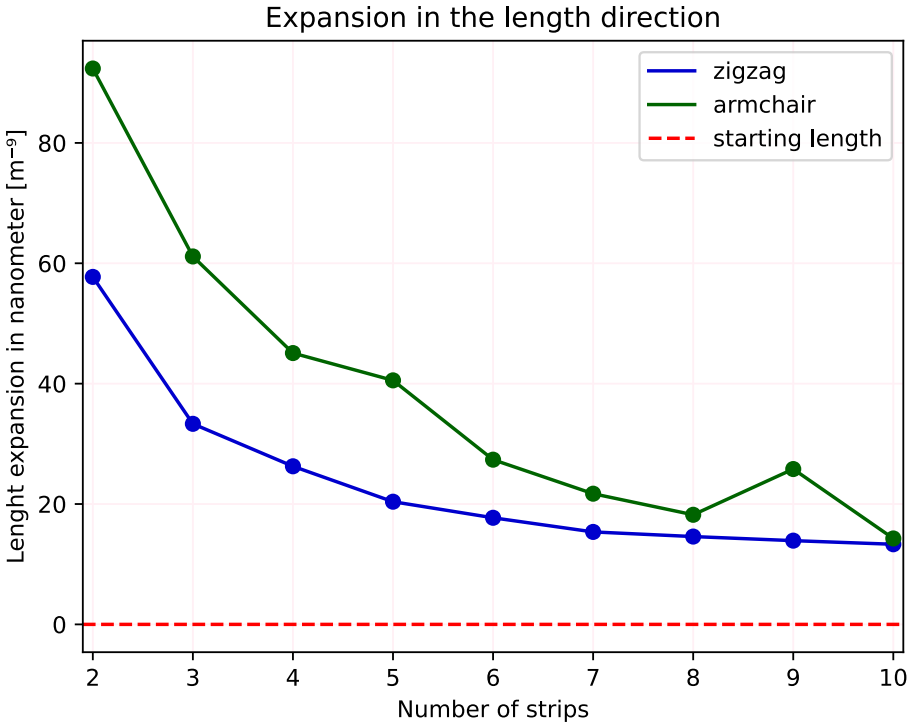


**Figure 4.11:** In this figure the total length expansion of the different ribbons is plotted. The red dotted line represent the initialized length of the ribbons. The blue and the green line represent how much the ribbons have grown in length during the simulation.

One very interesting observation can be made when looking at figure 4.11 and 4.10 and taking note of the fact that the bond-length in the length direction decreases dramatically at the same time as the lenght of the ribbons increases when going from 3 strip ribbons to 2 strip ribbons. This is true for both configurations of the ribbon. This can only happen if the honeycomb structures becomes deformed, and the angles of the bonds change.

# Chapter 5

# Conclusion

In this thesis, Molecular Dynamics (MD) technique with the Approach to Equilibrium Method (AEMD) have been used to investigate how the thermal conductivity of graphene is affected by dimensionality, specifically, the effect of reducing the width dimension, $L_y$, of a 2D graphene nanoribbons (GNR) of side length, $L_x$, equal to $2\mu m$ until a quasi 1-dimensional sample is reached, i.e. $L_x >> L_y$. Throughout the work of this thesis more than 300 independent Molecular Dynamics simulations have been completed, more than 50 gigabytes of unique data has been generated, 4037 lines of python code has been written, and most of the figures I have used have been created by myself using Inkscape. In addition to this, every Molecular Dynamics simulation of graphene nanoribbons presented in the results of this thesis, have had their output data files inspected using OVITO (Open VIsualization TOol), to verify that there are no defects along the edges of the ribbons. In the thesis, there are the results for 20 GNR , 10 A-GNR and 10-GNR. However, I have also inspected many ribbons that turned out to have defects and other technically problems, so the real number of simulation performed is actually much larger.

I have learned how to use the Approach to Equilibrium method to run Molecular Dynamics simulations of graphene that successfully reproduced data from previous work by Barbarino [8][22]. In addition to successfully reproducing the data, I have also been able to reproduce the temperature profile of AEMD simulations as it is reported in [6][7][22]. I have optimized the simulation-time from the 2-3 days it took at the start of this thesis work, to now being able to run them in 3 hours using the full performance available on NTNU's physics departments server called HPC-2.

The first part of the main result of this thesis is that the thermal conductivity of A-GNR, see 3.9, is decreasing as the graphene ribbon strips are ripped out from the initial 9 hexagonal layers or 10 strips configuration of hexagonal structures to just the 1 hexagonal layer (2 strips) configuration. This is not a simple linear function, but this could be due also to average issue. The thermal conductivity decreases by 27.7% from the 10-strips configuration to the 2-strip.

The second part of the main result of this thesis is that for nanoribbons in the

zigzag configuration 3.10, the thermal conductivity increases as the ribbon goes from 9 hexagonal layers in the lateral direction (10 strips) to 1 hexagonal layer (2 strips). However, it is slightly decreasing from 9 layers to 5 layers, before it slowly increases so that 3 layers only has 3.4% lower thermal conductivity than the 9 layers. From 3 to 1 layers the thermal conductivity increases drastically, such that 1 layer has 99.0% higher thermal conductivity than the 9 layers ribbon.

Figure A.1 shows the comparison of the thermal conductivity for Armchair Graphene Nano Ribbons (A-GNR)and Zizag Graphene Nano Ribbons (Z-GNR) configurations against the number of strips. The graph clearly shows that the thermal conductivity of Z-GNR is higher than for the A-GNR configurations, similar conclusions and order of magnitude are presented into another Non equilibrium MD study [43] and mentioned in different experimental studies [24, 26].

I have also observed that both the configurations of the graphene nanoribbons increases in the direction of the gradient applied as the number of layers of hexagonal structures is reduced. This is an effect of the average length of the carbon-carbon bonds that increases when going from 9 layer ribbons to 2 layer ribbons. Drastically, the thermal conductivity decreases from 2 layer ribbons to the single layer ribbon. The only way both of these facts can be true is if the angles of the carbon-carbon bonds also changes a lot from the 2 layer ribbon to the 1 layer ribbon. Exactly how this change in angles happens, and why, could be something to explore in further work.

# Bibliography


[1] H. Lin, Q. Jian, X. Bai, D. Li, Z. Huang, W. Huang, S. Feng and Z. Cheng, 'Recent advances in thermal conductivity and thermal applications of graphene and its derivatives nanofluids,' *Applied Thermal Engineering*, vol. 218, p. 119 176, 2023.

[2] H. Zheng, M. Hao, R. Miao, J. Schaadt and C. Dames, 'Advances in thermal conductivity for energy applications: A review,' *Prog. Energy*, vol. 3, p. 012 002, 2021.

[3] L. S., *Thermal Transport in Low Dimensions*. Tiergartenstrasse 17, 69121 Heidelberg/Germany, 2016, vol. 921, ISBN: 978-3-319-29259-5. [Online]. Available: `https://www.springer.com/series/5304`.

[4] M. Sang, J. Shin, K. Kim and K. J. Yu, 'Electronic and thermal properties of graphene and recent advances in graphene-based electronics applications,' *Nanomaterials (Basel)*, vol. 9(3), p. 374, 2019.

[5] K. Novoselov, A. Geim, S. Morozov, D. Jiang, Y. Zhang, S. Dubonos, I. Grigorieva and A. Firsov, 'Electric field effect in atomically thin carbon films.,' *Science*, vol. 306, pp. 666–669, 2004.

[6] E. Lampin, P. Palla, P.-A. Francioso and C. F., 'Thermal conductivity from approach-to-equilibrium molecular dynamics,' *Journal of Applied Science*, vol. 114, p. 033 525, 2013.

[7] C. Melis and L. Colombo, 'Lattice thermal conductivity of si1xgex nanocomposites,' *Physical Review Letters*, vol. 112, p. 065 901, 2014.

[8] G. Barbarino, C. Melis and L. Colombo, 'Computer "intrinsic thermal conductivity in monolayer graphene is ultimately upper limited: A direct estimation by atomistic simulations.,' *Physical Review B*, vol. 91, p. 035 416, 2015.

[9] P. C. Hemmer, *Termisk Fysikk*, second. Tapir akademisk forlag, 2002, ISBN: 9788251917391.

[10] J. H. Lienhard IV and J. H. Lienhard V, *A Heat Transfer Textbook*, 5th. Mineola, NY: Dover Publications, Dec. 2019, 784 pp., ISBN: 9780486837352. [Online]. Available: `http://ahtt.mit.edu`.

[11] C. Kittel, *Introduction to Solid State Physics*, Eight. New York: John Wiley Sons, 2005, ISBN: 9780471415268.

[12] T. Wu S. Yan, Z. Kuai and W. Pan, 'Thermal conductivity enhancement on phase change materials for thermal energy storage: A review,' *Energy Storage Materials*, 2019.

[13] M. Simoncelli, N. Marzari and F. Mauri, 'Unified theory of thermal transport in crystals and glasses,' *Nature Physics*, vol. 15, no. 8, pp. 809–813, 2019.

[14] T. M. Tritt, *Thermal conductivity: theory, properties, and applications*. Springer Science & Business Media, 2005.

[15] A. J. McGaughey and M. Kaviany, 'Phonon transport in molecular dynamics simulations: Formulation and thermal conductivity prediction,' *Advances in heat transfer*, vol. 39, pp. 169–255, 2006.

[16] A. A. Balandin, S. Ghosh, W. Bao, I. Calizo, T. D., F. Miao and C. N. Lau, 'Superior thermal conductivity of single-layer graphene,' *Nano Letters*, vol. 8, no. 3, pp. 902–907, 2008.

[17] A. A. Balandin, 'Thermal properties of graphene and nanostructured carbon materials,' *Nature materials*, vol. 10, no. 8, pp. 569–581, 2011.

[18] S. Chen, Q. Wu, C. Mishra, J. Kang, H. Zhang, K. Cho, W. Cai, A. Balandin and R. Ruoff, 'Thermal conductivity of isotopically modified graphene,' *Nature Materials*, vol. 10, no. 3, 2012.

[19] X. Xu, L. F. Pereira, Y. Wang, J. Wu, K. Zhang, X. Zhao, S. Bae, C. Tinh Bui, R. Xie, J. T. Thong *et al.*, 'Length-dependent thermal conductivity in suspended single-layer graphene,' *Nature communications*, vol. 5, no. 1, p. 3689, 2014.

[20] S. Ghosh, W. Bao, D. Nika, S. Subrina, E. Pokatilov, C. Lau and A. Balandin, 'Dimensional crossover of thermal transport in few-layer graphene,' *Nature Materials*, vol. 9, no. 7, pp. 555–558, 2010.

[21] T. J. Vlugt, J. P. van der Eerden, M. Dijkstra, B. Smit and D. Frenkel, *Introduction to Molecular Simulation and Statistical Thermodynamics*. Delft, The Netherlands, 2008, ISBN: 978-90-9024432-7. [Online]. Available: `http://www.phys.uu.nl/%E2%88%BCvlugt/imsst`.

[22] G. Barbarino, 'Thermal properties of graphene and graphene-based thermal diodes: A molecular dynamics study,' Ph.D. dissertation, Universita' degli studi di Cagliari, Dipartimento di Fisica, 2016.

[23] S. Dutta and S. K. Pati, 'Novel properties of graphene nanoribbons: A review,' *Journal of Materials Chemistry*, vol. 20, no. 38, pp. 8207–8223, 2010.

[24] K. He, G.-D. Lee, A. W. Robertson, E. Yoon and J. H. Warner, 'Hydrogen-free graphene edges,' *Nature communications*, vol. 5, no. 1, p. 3040, 2014.

[25] J. Hu, X. Ruan and Y. P. Chen, 'Thermal conductivity and thermal rectification in graphene nanoribbons: A molecular dynamics study,' *Nano letters*, vol. 9, no. 7, pp. 2730–2735, 2009.

[26] J. Chen and B. Liu, 'Dimension-dependent thermal conductivity of graphene nanoribbons on silicon carbide,' *The European Physical Journal Plus*, vol. 136, no. 4, p. 379, 2021.

[27] J. H. Seol, I. Jo, A. L. Moore, L. Lindsay, Z. H. Aitken, M. T. Pettes, X. Li, Z. Yao, R. Huang, D. Broido *et al.*, 'Two-dimensional phonon transport in supported graphene,' *Science*, vol. 328, no. 5975, pp. 213–216, 2010.

[28] M. Park, S.-C. Lee and Y.-S. Kim, 'Length-dependent lattice thermal conductivity of graphene and its macroscopic limit,' *Journal of Applied Physics*, vol. 114, no. 5, 2013.

[29] C. Yu and G. Zhang, 'Impacts of length and geometry deformation on thermal conductivity of graphene nanoribbons,' *Journal of Applied Physics*, vol. 113, no. 4, 2013.

[30] Y. Sheng, Y. Hu, Z. Fan and H. Bao, 'Size effect and transient phonon transport mechanism in approach-to-equilibrium molecular dynamics simulations,' *Physical Review B*, vol. 105, no. 7, p. 075 301, 2022.

[31] M. Allen, D. Tildesley and D. Tildesley, *Computer Simulation of Liquids* (Oxford science publications). Oxford University Press, 2017, ISBN: 9780198803195. [Online]. Available: https://books.google.no/books?id=nlExDwAAQBAJ.

[32] D. Frenkel and B. Smit, *Understanding Molecular Simulation: From Algorithms to Applications* (Computational Science Series), Second. San Diego: Academic Press, 2002, vol. 1.

[33] L. Verlett, 'Computer "experiments" on classical fluids. i. thermodynamical properties of lennard-jones molecules*,' *Physical Review*, vol. 159, no. 1, pp. 98–103, 1967.

[34] D. Levesque and L. Verlett, 'Pertubation theory and equation of state for fluids,' *Physical Review*, vol. 182, no. 1, pp. 307–316, 1969.

[35] W. J. Parker, R. J. Jenkins, C. P. Butler and G. L. Abbott, 'Flash Method of Determining Thermal Diffusivity, Heat Capacity, and Thermal Conductivity,' *Journal of Applied Physics*, vol. 32, no. 9, pp. 1679–1684, Jun. 2004, ISSN: 0021-8979. DOI: 10.1063/1.1728417. eprint: https://pubs.aip.org/aip/jap/article-pdf/32/9/1679/7929744/1679_1_online.pdf. [Online]. Available: https://doi.org/10.1063/1.1728417.

[36] J. D. Schall, P. T. Mikulski, K. E. Ryan, P. L. Keating, M. T. Knippenberg and J. A. Harrison, 'Reactive empirical bond-order potentials,' in *Encyclopedia of Nanotechnology*, B. Bhushan, Ed. Dordrecht: Springer Netherlands, 2012, pp. 2210–2221, ISBN: 978-90-481-9751-4. DOI: 10.1007/978-90-481-9751-4_399. [Online]. Available: https://doi.org/10.1007/978-90-481-9751-4_399.

[37] G. C. Abell, 'Empirical chemical pseudopotential theory of molecular and metallic bonding,' *Phys. Rev. B*, vol. 31, pp. 6184–6196, 10 May 1985. DOI: 10.1103/PhysRevB.31.6184. [Online]. Available: https://link.aps.org/doi/10.1103/PhysRevB.31.6184.

[38] J. Tersoff, 'New empirical approach for the structure and energy of covalent systems,' *Phys. Rev. B*, vol. 37, pp. 6991–7000, 12 Apr. 1988. DOI: 10.1103/PhysRevB.37.6991. [Online]. Available: https://link.aps.org/doi/10.1103/PhysRevB.37.6991.

[39] D. W. Brenner, 'Empirical potential for hydrocarbons for use in simulating the chemical vapor deposition of diamond films,' *Phys. Rev. B*, vol. 42, pp. 9458–9471, 15 Nov. 1990. DOI: 10.1103/PhysRevB.42.9458. [Online]. Available: https://link.aps.org/doi/10.1103/PhysRevB.42.9458.

[40] D. Brenner, O. Shenderova, J. Harrison, S. Stuart, B. Ni and S. Sinnott, 'A second-generation reactive empirical bond order (rebo) potential energy expression for hydrocarbons,' *J. Phys.: Condens. Matter*, vol. 14, pp. 783–802, Feb. 2002. DOI: 10.1088/0953-8984/14/4/312.

[41] N. Wei, L. Xu, H.-Q. Wang and J.-C. Zheng, 'Strain engineering of thermal conductivity in graphene sheets and nanoribbons: A demonstration of magic flexibility,' *Nanotechnology*, vol. 22, no. 10, p. 105 705, Feb. 2011. DOI: 10.1088/0957-4484/22/10/105705. [Online]. Available: https://dx.doi.org/10.1088/0957-4484/22/10/105705.

[42] X. Wu, V. Varshney, J. Lee, Y. Pang, A. K. Roy and T. Luo, 'How to characterize thermal transport capability of 2d materials fairly? sheet thermal conductance and the choice of thickness,' *Chemical Physics Letters*, vol. 669, pp. 233–237, 2017, ISSN: 0009-2614. DOI: https://doi.org/10.1016/j.cplett.2016.12.054. [Online]. Available: https://www.sciencedirect.com/science/article/pii/S0009261416310193.

[43] Z. Guo, D. Zhang and X.-G. Gong, 'Thermal conductivity of graphene nanoribbons,' *Applied physics letters*, vol. 95, no. 16, 2009.

# Appendix A

# Appendix

## A.1 $k$ plotted for 1-10 strips of both armchair and zigzag.

Figure A.1 shows the comparison of the thermal conductivity for Armchair Graphene Nano Ribbons (A-GNR)and Zizag Graphene Nano Ribbons (Z-GNR) configurations against the number of strips. The 1 strip cases looses their structure since they have no complete hexagonal structures, and thus limited rigidity. The monoatomic chains they turn into, have a lot higher $k$ values than the ribbons, thus blowing up the y-axis and making other details of the plots hard to see. Because of this it is only presented in the appendix.

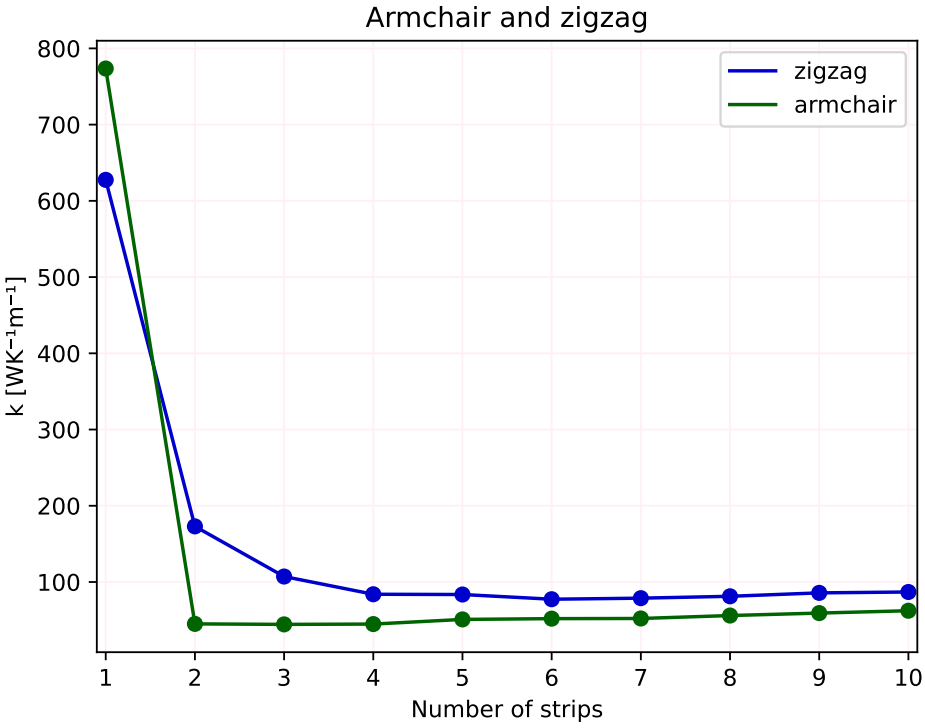


**Figure A.1:** Thermal conductivity against number of strips. Those data have been extracted from simulations of $2\mu m$ long ribbons of graphene in the armchair and the zigzag edge-configuration.

## A.2 Thermal diffusivity $\bar{k}$ for armchair simulations

The initialized length of all strips in the armchair configuration was 2016.4$nm$. As the system is heated up and equilibrated, this length changes. The numbers presented in this table are the lengths calculated along the ribbons in its final configuration at the end of the simulation. Details of how this was done is covered in chapter 3.6.3.

| # of strips | $\bar{k}[m^2s^{-1}]$ | Uncertainty | Length $[nm]$ |
|---|---|---|---|
| 1 | 131.432 | ±0.2506 | 2532.38 |
| 2 | 4.6156 | ±0.0013 | 2074.10 |
| 3 | 4.4942 | ±0.0008 | 2049.68 |
| 4 | 4.5208 | ±0.0008 | 2042.63 |
| 5 | 5.1227 | ±0.0009 | 2036.74 |
| 6 | 5.2176 | ±0.0006 | 2034.07 |
| 7 | 5.2327 | ±0.0007 | 2031.72 |
| 8 | 5.6187 | ±0.0007 | 2030.95 |
| 9 | 5.9389 | ±0.0008 | 2030.27 |
| 10 | 6.2477 | ±0.0007 | 2029.67 |

Each strip in the armchair configuration consists of 18960 atoms.

## A.3 Thermal diffusivity $\bar{k}$ for zigzag simulations

The initialized length of all strips in zigzag configuration was 2004.1$nm$. As the system is heated up and equilibrated, this length changes. The numbers presented in this table are the lengths calculated along the ribbons in its final configuration at the end of the simulation. Details of how this was done is covered in chapter 3.6.3.

| # of strips | $\bar{k}[m^2s^{-1}]$ | Uncertainty | Length $[nm]$ |
|---|---|---|---|
| 1 | 105.577 | ±0.2176 | 2158.35 |
| 2 | 18.0216 | ±0.0196 | 2096.50 |
| 3 | 11.001 | ±0.0062 | 2065.27 |
| 4 | 8.5462 | ±0.0031 | 2049.22 |
| 5 | 8.4928 | ±0.0018 | 2044.68 |
| 6 | 7.8155 | ±0.0023 | 2031.50 |
| 7 | 7.9321 | ±0.0016 | 2025.85 |
| 8 | 8.1643 | ±0.0016 | 2022.35 |
| 9 | 8.6489 | ±0.0017 | 2029.94 |
| 10 | 8.7147 | ±0.0019 | 2018.41 |

Each strip in the zigzag configuration consists of 16320 atoms.

## A.4 Final configuration of 1 strip armchair ribbon

In figure A.2 the final configuration of the 1 strip armchair configuration can be seen. Since this strip is only 1 atom wide and 18960 atoms long, it is hard to see the details when it is this small. However, it is still possible to get some idea of the general shape. There are no places where a carbon atom is bound to more than 2 atoms. Some places where it looks like this is the case, it is just an artifact of the shape moving in or out of the plane of the paper. This has been verified by examining the strip in 3 dimensions by use of the visualisation software OVITO.

**Figure A.2:** This is a screenshot from OVITO showing the end configuration of a single armchair strip after a full AEMD simulation. The details are very hard to see with this resolution, however it is possible to get some idea of the general shape

## A.5 REBO performance on hybrid architecture CPU

At the time of writing this masters thesis hybrid architecture CPU's is a fairly new technology in x86 based systems. Hybrid architecture in Intel based systems currently has the CPU built up by two different types of cores, the performance cores (P-cores) and the efficiency cores (E-cores).

The P-cores are physically larger than the E-cores, runs at higher clock speed and supports turbo, i.e. they clock to higher clock speeds if there is thermal headroom. In addition the P-cores have support for Hyper-Threading, which means they are able to run 2 threads at once. In short the P-cores are designed to maximize instructions per cycle inside the thermal limits of the CPU.

E-cores are built different and are smaller on the chip, run lower clocks and are in general designed to maximize performance per watt. This means they are a lot slower than E-cores, but they can still help accelerate workloads that are core-hungry.

To test how well MD simulations of the REBO potential runs on a hybrid architecture CPU, I built a 8 strip AGNR that was $2\mu m$ long, and ran the first 5000 steps of my implementation of the AEMD method on a Intel 13900KS CPU. As of writing this thesis, the 13900KS is the highest performance consumer CPU offered by Intel. This CPU can run up to 32 threads at once, so I had to repeat the test 32 times, using the omp flag in LAMMPS to add one extra CPU-thread each time I ran the simulation.

The results can be seen in figure A.3. It is clear that the simulation speed scales well while adding the 8 P-cores. Adding the next 16 E-cores has roughly the same scaling as adding 4 P-cores, so scaling on E-cores is not great. The scaling is negative when adding extra threads to the P-cores by utilizing Hyper-Threading. This is due to the threads doing very similar calculations, thus ending up waiting for the same resources on the P-core instead of being simulated at the same time.

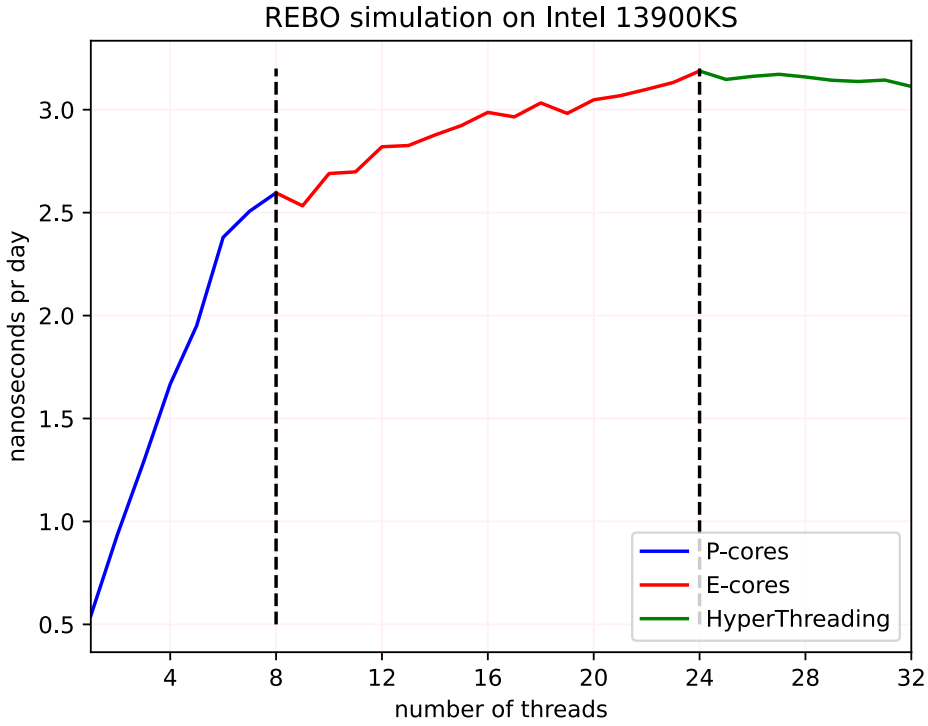


**Figure A.3:** Simulation of a 8 strip AGNR consisting of 151680 atoms using the REBO potential and the omp accelerator package, on an Intel 13900KS processor. P-cores are the performance cores in the CPU while E-cores are the efficiency cores. Hyper-Threading is the second thread that can be run in each of the P-cores.

## A.6 Effect of using the "omp" flag in LAMMPS when running simulations with SLURM

The HPC-2 server I used for most of my simulations ran the SLURM workload manager. To run a job on this server a job script has to specify the partition the job is to be run on, how many of the partitions nodes should be used, how many tasks should be run per node, how many CPU's should be used per task, what file should be run, and so on.

It is the Message Passing Interface (MPI) standard that is used when the number of tasks per node is set. This divides the nodes resources equally among the tasks, i.e a node with 20 CPU's and 100 GB memory running 2 tasks will be set up in such a way that each task always has 10 CPU's and 50 GB memory available.

When "CPU's per task" is set, this is set by the OpenMP standard which shares the resources between the running threads. If we continue the last example and say that the job script asking for "2 tasks per node" also asks for "8 CPU's per task"

then the 20 CPU, 100GB memory node will be divided into two groups of 10 CPU's and 50GB, and each of the task will use 8 out its 10 available CPU's. These 8 CPU's will share the 50GB of memory that is allocated to the task by the MPI.

When all of this can be set in the job script in SLURM a natural question (at least for someone learning this) is **what effect does the omp flag in LAMMPs have when running jobs where the number of CPU's per task (omp), and number of tasks per node (ntask), is already defined?**

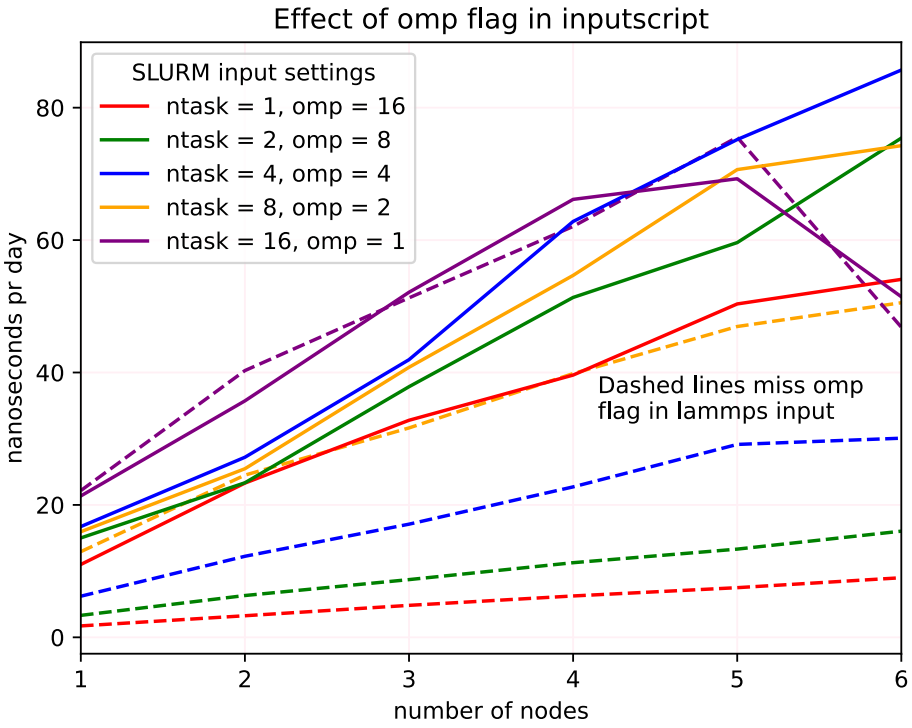


**Figure A.4:** The lines of the same color was run with the same settings for ntask and "cpu per task" (omp) in the SLURM job script. The difference between them is that the dashed lines are from LAMMPS inputs without the omp accelerator package activated, while the solid lines have omp flag in their LAMMPS script. Other than that they are identical.

The answer can be seen in figure A.4 which tells us that if a job in SLURM is set to run as multiple tasks, then LAMMPS will run in parallel without the need for any flags in the input script. However, if the job in SLURM also asks that each task should use more than 1 CPU, then the presence of the omp flag in LAMMPS has a massive impact on the performance. When the omp flag is activated in a LAMMPS input script, it should always be set to ask for the same number of omp as the SLURM job script asks for in the "CPU's per task" line.